

Electronic Supplementary Information

Theoretical and Experimental Exploration on NiM(111) (**M** = Fe, Co, Cu, Zn) Bimetallic Catalysts for Water-Gas Shift Reaction

Pan Yin,^a Hao Meng,^a Lei Wang,^a Yingjie Lai,^a Yao Jie,^a Jun Yu,^a Wei Liu,^a Xiaojie Zhao,^a

Tianyao Shen,^a Xin Zhang,^a Jingbin Han,^a Yusen Yang,^{*a} Hong Yan,^{*a} and Min Wei^a

^a State Key Laboratory of Chemical Resource Engineering, College of Chemistry, Beijing University of Chemical Technology, Beijing 100029, China

* Corresponding Authors:

yangyusen@mail.buct.edu.cn (Yusen Yang); yanhong@mail.buct.edu.cn (Hong Yan).

CONTENTS

Title	Page
1. Computational models (Fig. S1-S4, Table S1-S8)	S3
2. Reaction paths and mechanisms (Fig. S5)	S8
3. Theoretical methods	S10
4. Adsorption site test (Table S9, Fig. S6-S10)	S13
5. The size and the average charge of adsorption sites (Table S10, Fig. S11-S13)	S18
6. Adsorption of H ₂ O and CO on Fe(110), Co(111), Cu(111) and Zn(001) surfaces (Fig. S14-S15, Table S11)	S21
7. WGSR elementary reaction step on NiCo(111) and NiCu(111) surfaces (Fig. S16-S17, Table S12)	S24
8. Microkinetic modeling analysis of WGS reaction (Table S13-S22, Fig. S18)	S27
9. Experimental details (Fig. S19-S20)	S37
10. References	S39

1. Computational models

In this work, before constructing the surface model, the lattice parameters of bulk Ni, bulk M (M = Fe, Co, Cu, Zn) and NiM bimetallic are calculated. Ni catalyst is constructed according to XRD data (XRD standard cards: Ni-PDF#04-0850, face-centered cubic (fcc), lattice parameters $a = b = c = 3.52 \text{ \AA}$, $\alpha = \beta = \gamma = 90^\circ$). Fe catalyst is constructed according to XRD data (XRD standard cards: Fe-PDF#34-0529, triclinic, lattice parameters $a = b = c = 2.83 \text{ \AA}$, $\alpha = \beta = \gamma = 90^\circ$). Co catalyst is constructed according to XRD data (XRD standard cards: Co-PDF#15-0806, fcc, lattice parameters $a = b = c = 3.53 \text{ \AA}$, $\alpha = \beta = \gamma = 90^\circ$). Cu catalyst is constructed according to XRD data (XRD standard cards: Cu-PDF#04-0836, fcc, lattice parameters $a = b = c = 3.64 \text{ \AA}$, $\alpha = \beta = \gamma = 90^\circ$). Zn catalyst is constructed according to XRD data (XRD standard cards: Zn-PDF#04-0831, triclinic, lattice parameters $a = b = 4.03 \text{ \AA}$, $c = 5.19 \text{ \AA}$, $\alpha = \beta = 90^\circ$, $\gamma = 120^\circ$). NiM bimetallic catalysts are optimized by adding the second metal element (Fe, Co, Cu and Zn) in equal proportions to replace Ni atoms of Ni cell.^{S1,S2} The calculated lattice parameters of the NiM alloy are (1) NiFe: fcc, $a = b = 3.57 \text{ \AA}$, $c = 3.58 \text{ \AA}$, $\alpha = \beta = \gamma = 90^\circ$; (2) NiCo: fcc, $a = b = 3.48 \text{ \AA}$, $c = 3.60 \text{ \AA}$, $\alpha = \beta = \gamma = 90^\circ$; (3) NiCu: fcc, $a = b = 3.56 \text{ \AA}$, $c = 3.57 \text{ \AA}$, $\alpha = \beta = \gamma = 90^\circ$; (4) NiZn: fcc, $a = b = 3.88 \text{ \AA}$, $c = 3.22 \text{ \AA}$, $\alpha = \beta = \gamma = 90^\circ$; respectively (**Fig. S1**). The Ni(111) and NiM(111) are cleaved from the optimized bulk Ni and NiM alloy (**Fig. 1**). For pure metal M surfaces, the most optimally exposed crystal surfaces are used for calculations (**Fig. S2**) Fe(110), Co(111), Cu(111), and Zn(001) surfaces are selected as reaction surface, since they have been reported to be favorable to expose.^{S3-S7} The surfaces are represented as $p(2\times 2)$ supercell with three-layer slabs, separated by 15 Å of vacuum.

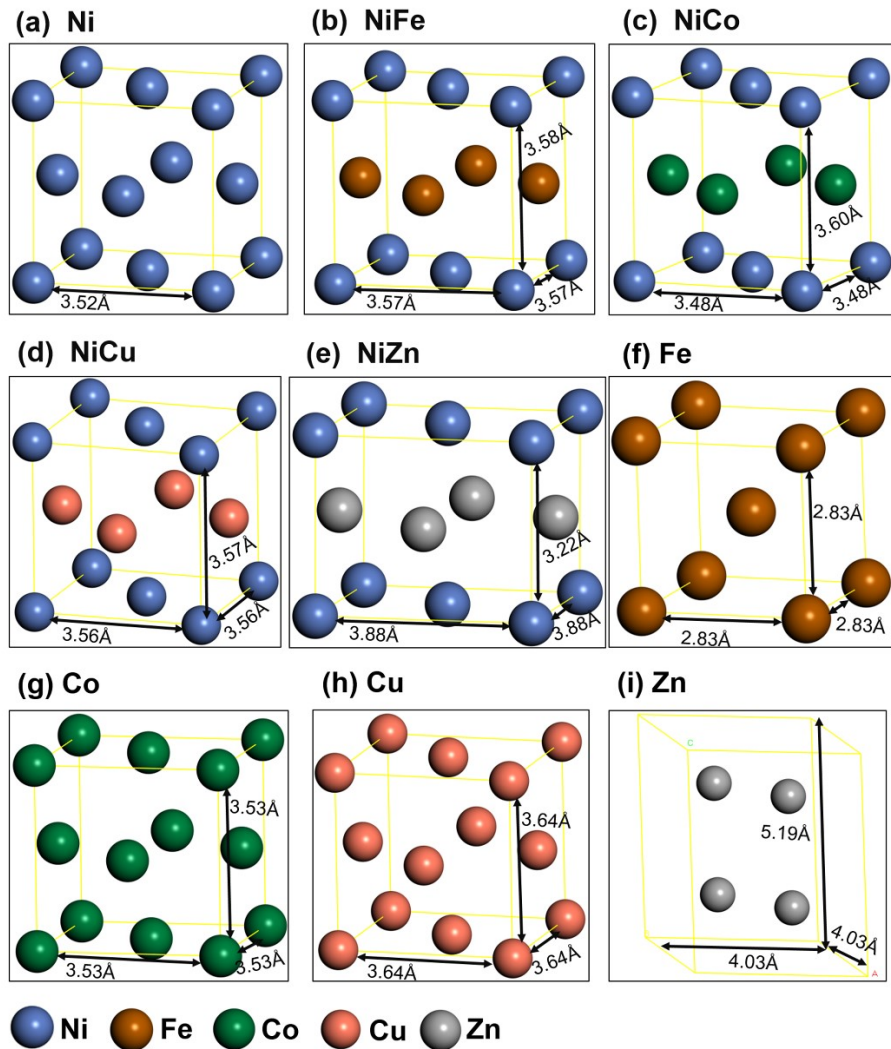


Fig. S1. Structure details of bulk Ni, bulk Fe , bulk Co , bulk Cu , bulk Zn , bulk NiFe, bulk NiCo, bulk NiCu and bulk NiZn.

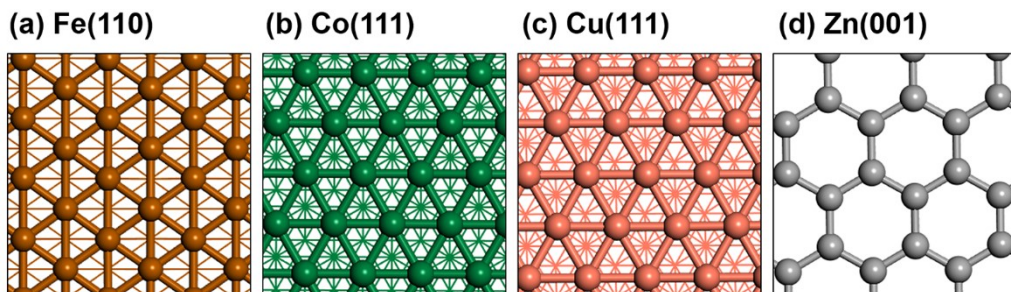


Fig. S2. The top view of the optimized structures of (a) Fe (110), (b) Co(111), (c) Cu(111) and (d) Zn(001) surfaces.

Table S1. Catalysts and their calculated properties

Catalyst	Atomic radius/ Å	ΔR	$\Delta E_b/\text{eV}$
Ni	Ni: $R_0=1.49$	0	–
NiFe	Fe: $R_1=1.56$	0.047	19.99
NiCo	Co: $R_2=1.52$	0.020	21.47
NiCu	Cu: $R_3=1.45$	-0.027	19.14
NiZn	Zn: $R_4=1.42$	-0.047	4.83

In order to test the supercell size of the calculation models, the models of Ni(111): (1) supercell 2×2 ; (2) supercell 3×3 ; (3) supercell 4×4 , with H_2O and CO absorbed, are optimized. The optimized structures are shown in **Fig. S3**. As shown, the adsorption energies of H_2O or CO on three different supercells are close to each other. Thus, in order to make rational use of computing resources, the models with 2×2 supercell are employed in this work.

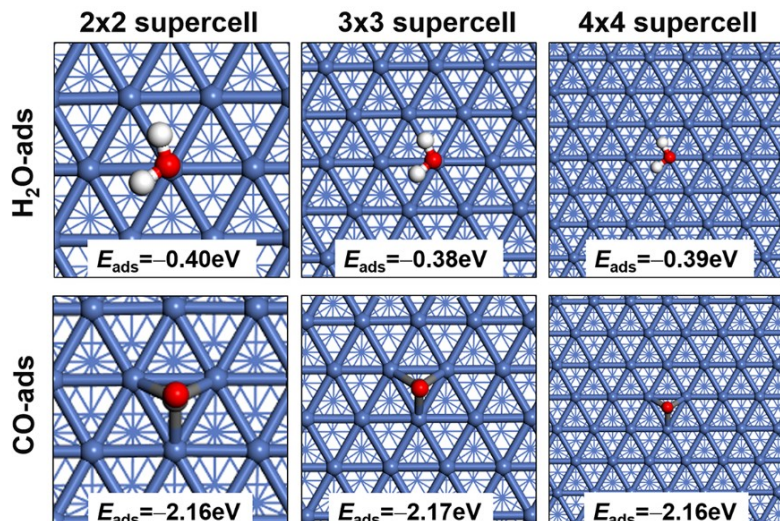


Fig. S3. The adsorption energies (E_{ads}) of H_2O and CO on 2×2 , 3×3 , 4×4 supercell of Ni(111) surfaces, respectively.

Table S2. A summary of the adsorption energy (E_{ads} , in eV) of related species (H_2O , H) for the WGS reaction on Ni(111) surface reported in the literature ($E_{\text{ads}}(\text{H})=E_{\text{total}}(\text{H})-(E_{\text{slab}}+E_g(\text{H atom}))$)

Ni(111)-Supercell	Method	$E_{\text{ads}}(\text{H}_2\text{O})$	$E_{\text{ads}}(\text{H})$	Reference
$p(2\times 2)$ unit cell	GGA-PBE	-0.40	-2.87	In this work
$p(2\times 2)$	GGA-PW91	-0.17	-2.83	<i>Science</i> 2014, 344 , 504

unit cell				
$p(2 \times 2)$ unit cell	GGA-PBE	-0.47	-2.77	<i>J. Phys. Chem. C</i> 2012, 116 , 20281
$p(2 \times 2)$ unit cell	GGA-PBE	-0.19	-2.65	<i>Surf. Sci.</i> 2016, 644 , 53
$p(3 \times 3)$ unit cell	GGA-PBE	-0.27	-2.80	<i>ChemCatChem</i> 2015, 7 , 3928
$p(3 \times 3)$ unit cell	GGA-RPBE	-	-2.64	<i>Appl. Catal. B-Environ.</i> 2020, 264 , 118430
$p(3 \times 3)$ unit cell	GGA-PBE	-0.16	-2.78	<i>ChemPhysChem</i> 2014, 15 , 2490

Table S3. Energies (E , in eV) of H species in the gas phase

Species	Energy/eV
$1/2\text{H}_2(\text{g})$	-3.38
H atom	-1.11

Fig. S4 and **Tables S4-S8** show the valence electrons of surface per atom on the Ni(111) and NiM(111) systems. The average valence electrons of Ni on the Ni(111), NiFe(111), NiCo(111), NiCu(111) and NiZn(111) surfaces are 10.00, 10.22, 10.10, 10.08 and 10.20, respectively.

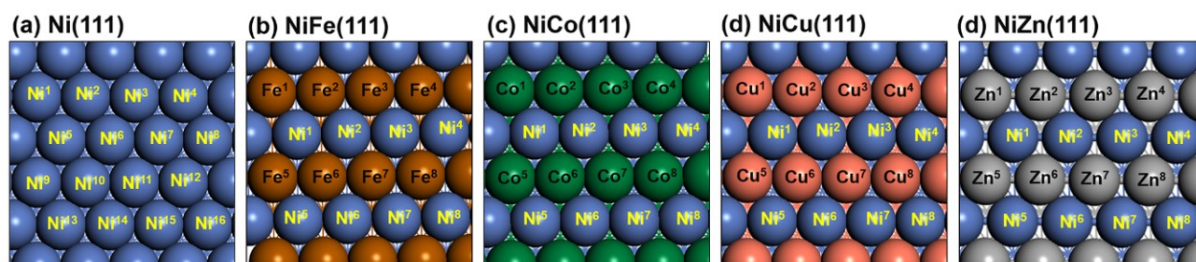


Fig. S4 Top view of the Ni(111) and NiM (111) surfaces models.

Table S4. Electron number of the outermost Ni atoms based on Bard charge analysis on the Ni(111) surface

Atom	Electron number	Atom	Electron number	Average
Ni ¹	10.01	Ni ⁹	10.03	10.00
Ni ²	10.02	Ni ¹⁰	10.02	

Ni ³	10.01	Ni ¹¹	10.02
Ni ⁴	10.03	Ni ¹²	10.01
Ni ⁵	10.01	Ni ¹³	9.97
Ni ⁶	9.98	Ni ¹⁴	10.03
Ni ⁷	10.01	Ni ¹⁵	9.98
Ni ⁸	9.99	Ni ¹⁶	10.01

Table S5. Electron number of the outermost Ni and Fe atoms based on Bard charge analysis on the NiFe(111) surface

Atom	Electron number	Averag e	Atom	Electron number	Averag e
Ni ¹	10.22		Fe ¹	7.82	
Ni ²	10.22		Fe ²	7.82	
Ni ³	10.22		Fe ³	7.82	
Ni ⁴	10.22	10.22	Fe ⁴	7.81	7.82
Ni ⁵	10.23		Fe ⁵	7.82	
Ni ⁶	10.22		Fe ⁶	7.81	
Ni ⁷	10.22		Fe ⁷	7.82	
Ni ⁸	10.21		Fe ⁸	7.82	

Table S6. Electron number of the outermost Ni and Co atoms based on Bard charge analysis on the NiCo(111) surface

Atom	Electron number	Averag e	Atom	Electron number	Averag e
Ni ¹	10.09		Co ¹	8.95	
Ni ²	10.11		Co ²	8.96	
Ni ³	10.10		Co ³	8.95	
Ni ⁴	10.09	10.10	Co ⁴	8.94	8.95
Ni ⁵	10.11		Co ⁵	8.95	
Ni ⁶	10.09		Co ⁶	8.94	
Ni ⁷	10.11		Co ⁷	8.95	
Ni ⁸	10.10		Co ⁸	8.96	

Table S7. Electron number of the outermost Ni and Cu atoms based on Bard charge analysis on the NiCu(111) surface

Atom	Electron number	Average	Atom	Electron number	Average
		e			e
Ni ¹	10.07		Cu ¹	10.96	
Ni ²	10.08		Cu ²	10.97	
Ni ³	10.07		Cu ³	10.96	
Ni ⁴	10.08		Cu ⁴	10.97	
Ni ⁵	10.08	10.08	Cu ⁵	10.96	10.97
Ni ⁶	10.07		Cu ⁶	10.97	
Ni ⁷	10.08		Cu ⁷	10.96	
Ni ⁸	10.07		Cu ⁸	10.97	

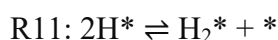
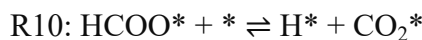
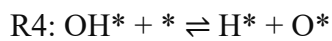
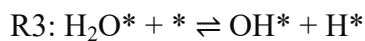
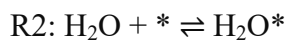
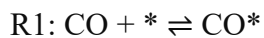
Table S8. Electron number of the outermost Ni and Zn atoms based on Bard charge analysis on the NiZn(111) surface

Atom	Electron number	Average	Atom	Electron number	Average
		e			
Ni ¹	10.18		Zn ¹	11.84	
Ni ²	10.19		Zn ²	11.82	
Ni ³	10.20		Zn ³	11.84	
Ni ⁴	10.21		Zn ⁴	11.85	
Ni ⁵	10.20	10.20	Zn ⁵	11.84	11.84
Ni ⁶	10.21		Zn ⁶	11.82	
Ni ⁷	10.20		Zn ⁷	11.84	
Ni ⁸	10.21		Zn ⁸	11.85	

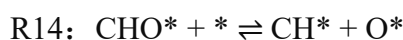
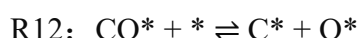
2. Reaction paths and mechanisms

There are three possible reaction paths^{S8,S9} for WGS (**Fig. S5**). The reactants CO and H₂O are adsorbed on the surfaces of the catalysts (R1 and R2), followed with the dissociation of H₂O (R3 and R4). In the redox mechanism, CO₂ is produced by the CO oxidization with O which is formed through

direct dissociation H₂O (R5). In the carboxyl mechanism, CO is oxidized by OH to COOH which dissociates to CO₂ directly (R6 and R7). In the formate mechanism, CO is oxidized by H to CHO and CHO is oxidized by O to HCOO which dissociates to CO₂ directly (R8, R9 and R10). Two H* bind each other to form hydrogen (R11). All elementary steps involved in WGS are listed as below.



R12 to R16 are the possible reactions for C–O bond breaking to C or CH intermediates, which are potential precursors of coke and methanation reactions and hinder the production of CO₂ and H₂.^{S10} The key steps that mainly affect the carbon deposition process are R12, R13 and R14, since these steps are relatively easy to occur.¹⁵





* represents a surface site, X* represents adsorption state.

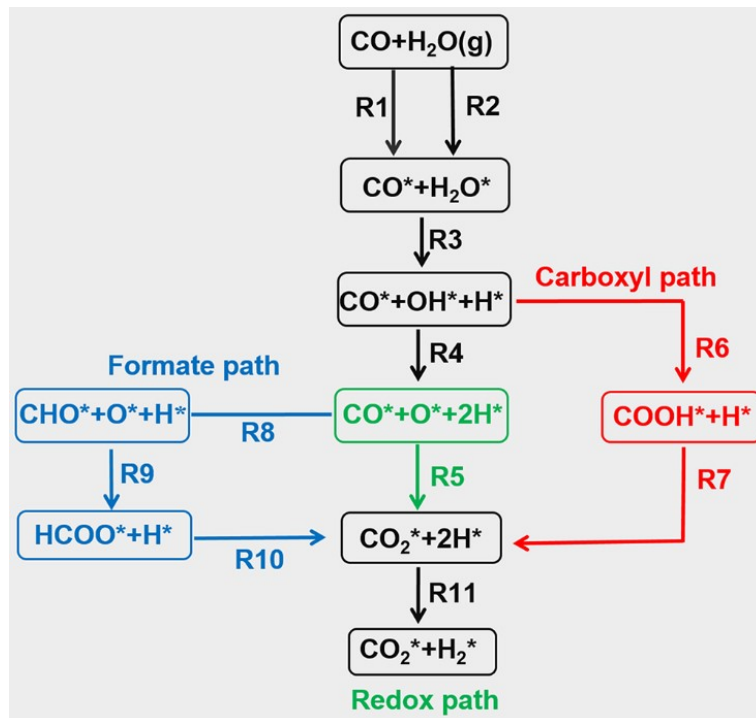


Fig. S5. Reaction paths of WGS reaction.

3. Theoretical methods

In this study, our calculations are based on spin-polarized density functional theory (DFT) within the exchange and correlation components of Perdew-Burke-Ernzerhof function (PBE) of the generalized gradient approximation (GGA) as implemented in the Vienna Ab Initio Simulation Package (VASP).^{S11-S14} The projector augmented wave (PAW) method with a plane wave basis set was employed to describe the interaction between ion cores and valence electrons.^{S15,S16} An energy cutoff of 500 eV was set for the expansion of the electronic eigenfunctions. The surfaces of bimetallic NiM catalysts were modeled as face-centered-cubic (fcc). All facets were modeled as slabs containing

three layers of 2×2 supercell. The bottom layer of the three-layered slab is fixed at corresponding bulk positions, the upper two layers were fully relaxed. For the Brillouin zone integration, we used a $(5\times 5\times 1)$ Monkhorst-Pack mesh of k-points to determine the optimal geometries and total energies of the systems. Transition state (TS) searches are performed at the same theoretical level with the CI-NEB method.^{S17,S18} The Bader charge and electron density difference are calculated to show the electron transfer between Ni and M elements on clean surfaces and electronic interactions between the NiM catalysts and adsorbates.

The adsorption energies (E_{ads}) of the species are calculated by the electronic energy difference between the surface containing the adsorbates (E_{total}) and the clean surface with the adsorbing molecule in gas phase ($E_{\text{slab}}+E_g$).

$$E_{\text{ads}} = E_{\text{total}} - (E_{\text{slab}} + E_g) \quad (\text{S1})$$

The energy barrier (E_a) is obtained from the electronic energy difference between the transition state (E_{TS}) and its corresponding initial state (E_{IS}), which defined as

$$E_a = E_{\text{TS}} - E_{\text{IS}} \quad (\text{S2})$$

Microkinetic modeling of WGS reaction over NiCo (111) and NiCu(111) surfaces are carried out to further study the coverages of the reactants (CO and H₂O) as a function of temperature and the ratio of initial pressure of H₂O(g) to CO(g) ($p_{\text{H}_2\text{O}}/p_{\text{CO}}$).

R1 and R2 are adsorption reactions, the rate constants of the reactants (CO and H₂O) are calculated as^{S19}

$$k_{\text{ads}}^i = s_0 p_i A / \sqrt{2\pi m_i k_B T} \quad (\text{S3})$$

Wherein sticking coefficient (s_0) for H₂O and CO are set as 0.75 and 0.84^{S20}; k_B is the Boltzmann constant, 1.381×10^{-23} J·K⁻¹; the value of temperature (T) ranges from 423 K to 723 K; p_i is the partial

pressure (in Pa) of H₂O or CO, the total pressure is keeping as 100 kPa, five different ratios (1:1; 4:1; 9:1; 14:1; 19:1) of $p_{\text{H}_2\text{O}}/p_{\text{CO}}$ are calculated; m_i is molecular mass of species i (kg); the A is the area of adsorption site (m²), A of Ni is set as 4.88×10^{-20} m² and A of Co is set as 4.99×10^{-20} m².^{S21}

The adsorption reactions of CO and H₂O (R1 and R2) are assumed to be in equilibrium, the equilibrium constants were defined as follow^{S22}:

$$K = \exp[-(E_{\text{ads}} - T\Delta S)/k_B T] \quad (\text{S4})$$

Wherein E_{ads} refers to the adsorption energy of CO or H₂O, k_B is the Boltzmann constant, T is the operating temperature, and ΔS is the entropy change from the gas phase at the operating temperature. The rate constant of (k_{des}) of the desorption process (the reverse reaction of R1 and R2) is calculated according to the formula of $k_{\text{des}} = k_{\text{ads}}^i / K$.

For R3-R6, the pre-exponential factors for the forward (v_{for}) and reverse reaction step (v_{rev}) are obtained by the vibrational frequencies of initial state and transition state, and the vibrational frequencies of final state and transition state, respectively.^{S22}

$$v_{\text{for}} = \prod_{i=1}^N v_i^{\text{IS}} / \prod_{j=1}^{N-1} v_j^{\text{TS}} \quad (\text{S5})$$

$$v_{\text{rev}} = \prod_{i=1}^N v_i^{\text{FS}} / \prod_{j=1}^{N-1} v_j^{\text{TS}} \quad (\text{S6})$$

N represents the number of frequencies and depends on the degree of freedom of the molecule; v_i and v_j are the frequencies of species of the initial state and the transition state in a certain elementary step, respectively.

The free energies (G) are calculated by

$$G = E_{\text{elec}} + E_{\text{ZPE}} - TS \quad (\text{S7})$$

wherein E_{elec} is the total electronic energy of the interface at 0 K; E_{ZPE} is the zero-point vibrational energy, only the vibration entropy (S_{vib}) is taken into account.^{S23}

Entropy is obtained from the standard vibrational entropy (S_{vib}°) by^{S24}

$$S_{\text{vib}}^{\circ} = R \sum_i \left\{ \frac{hc\nu_i / k_B T}{e^{hc\nu_i / k_B T} - 1} \cdot \ln \left(1 - e^{-hc\nu_i / k_B T} \right) \right\} \quad (\text{S8})$$

where R is gas molar constant; k_B is the Boltzmann constant; h is the Planck constant; c is the light speed, and ν_i is the wavenumber.

Then the rate constant (k_i) of the elementary step i is calculated as

$$k = v_{\text{for/rev}} \exp(-\Delta G / RT) \quad (\text{S9})$$

wherein ΔG is the free energy of activation, $\Delta G = E_a + \Delta \text{ZPE} - T\Delta S$.

To investigate the reactivity on NiM surfaces, the d-band center, which has been widely used for predicting the reactivity trend on metal surfaces using DFT calculations is calculated.^{S25,S26} According to Nørskov's study, the occupied d-band center ε_d is calculated by equation^{S25}

$$\varepsilon_d = \frac{\int_{-\infty}^{E_f} E \rho_d(E) dE}{\int_{-\infty}^{E_f} \rho(E) dE} \quad (\text{S10})$$

where ρ_d is the projected density of states (PDOS) of the d-band of surface atoms, and E_f is the Fermi level energy.

4. Adsorption site test

The possible adsorption sites of Ni (111) and NiM(111) surfaces are shown in **Fig. S6**. In general, there are three high-symmetry adsorption sites on Ni(111), *i.e.*, top site above a surface atom, bridge site coordinated simultaneously to two adjacent surface atoms, and 3-fold hollow site formed by three adjacent atoms (**Fig. S6a**). Compared with the Ni(111) surface, the adsorption sites of the NiM(111) (M=Fe, Co, Cu, Zn) surface are more multifarious, including two types of top sites, three types of bridge sites, and two types of 3-fold sites (**Fig. S6b-e**). The two types of top sites are t-Ni and t-M

(M=Fe, Co, Cu, Zn), which are directly above Ni and M (M=Fe, Co, Cu, Zn) atoms. The bridge sites can be formed by two adjacent Ni atoms (b-Ni₂), one Ni and one adjacent M atom (b-NiM), and two adjacent M atoms (b-M₂). The 3-fold sites can be formed by two Ni atoms with one M atom (h-Ni₂M) and one Ni atom with two M atoms (h-NiM₂). All of these adsorption sites are taken into consideration in the adsorptions of species involved in WGS on the Ni(111) and NiM(111) surfaces.

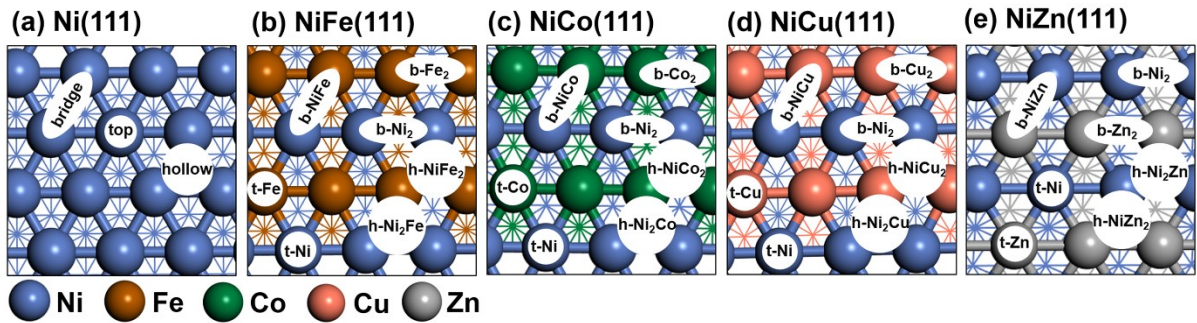


Fig. S6. The schematic of the adsorption sites of (a) Ni (111), (b) NiFe(111), (c) NiCo(111), (d) NiCu(111), (e) NiZn(111) surfaces. The numbers (in e) are the valence electrons by Bader charge analyses. (Ni: blue; Fe: maroon; Co: green; Cu: light brown; Zn: grey; O: red; H: white; C: dark gray).

Table S9. Adsorption energies (E_{ads} , in eV) and bond distance (d , in Å) between species and surface atoms involved in the WGS reaction on Ni(111) and NiM(111)

	Species	H ₂ O	CO	OH	H	H ₂	CO ₂
Ni(111)	site	t-Ni	h-Ni ₃	h-Ni ₃	h-Ni ₃	t-Ni	b-Ni ₂
	E_{ads}	-0.40	-2.16	-3.24	-2.87	-0.39	-0.15
	d	2.16	1.94/1.94/1.95	1.95/1.95/1.96	1.69/1.69/1.69	1.58	1.94/1.92
NiFe(111)	site	t-Fe	h-FeNi ₂	h-FeNi ₂	h-FeNi ₂	h-FeNi ₂	h-FeNi ₂
	E_{ads}	-0.39	-1.80	-3.63	-2.85	-0.27	-0.04
	d	2.20	2.03/2.08/1.94	2.02/2.01/2.05	1.71/1.79/1.79	1.65	2.30/1.97/2.27
NiCo(111)	site	t-Co	h-Ni ₂ Co	h-CoNi ₂	h-CoNi ₂	t-Co	b-Co ₂
	E_{ads}	-0.35	-1.74	-3.58	-2.75	-0.30	0.34
	d	2.21	1.99/2.03/1.90	1.99/1.99/2.00	1.71/1.75/1.75	1.62	2.24/2.01
NiCu(111)	site	t-Ni	b-Ni ₂	h-CuNi ₂	h-CuNi ₂	t-Ni	t-Ni
	E_{ads}	-0.32	-1.95	-3.19	-2.68	-0.36	-0.05

	<i>d</i>	2.18	1.88/1.88	1.94/2.04/2.05	1.64/1.78/1.79	1.60	3.68
	site	t-Ni	b-Ni ₂	h-Ni ₂ Zn	b-Ni ₂	t-Ni	h-Ni ₂ Zn
NiZn(111)	<i>E</i> _{ads}	-0.22	-1.68	-3.35	-2.81	-0.37	0.22
	<i>d</i>	2.24	1.91/1.91	2.02/2.03/2.06	1.67/1.67	1.59	1.93/2.03/2.20

In order to find the most stable structures of all the species involved in the mechanism (H_2O , H_2 , OH, O, H, CO, CO_2 , COOH, CHO and HCOO) on NiFe(111), NiCo(111), NiCu(111) and NiZn(111) surfaces, several possible adsorption sites are tested. The most stable adsorption structures of H_2O , OH, H, CO, CHO, CH and C are the t-Fe site, h-NiFe₂ site, h-Ni₂Fe site, h-NiFe₂ site, h-NiFe₂ site, h-Ni₂Fe site and h-Ni₂Fe site on the NiFe(111) surface, respectively, as highlighted in red in **Fig. S7**.

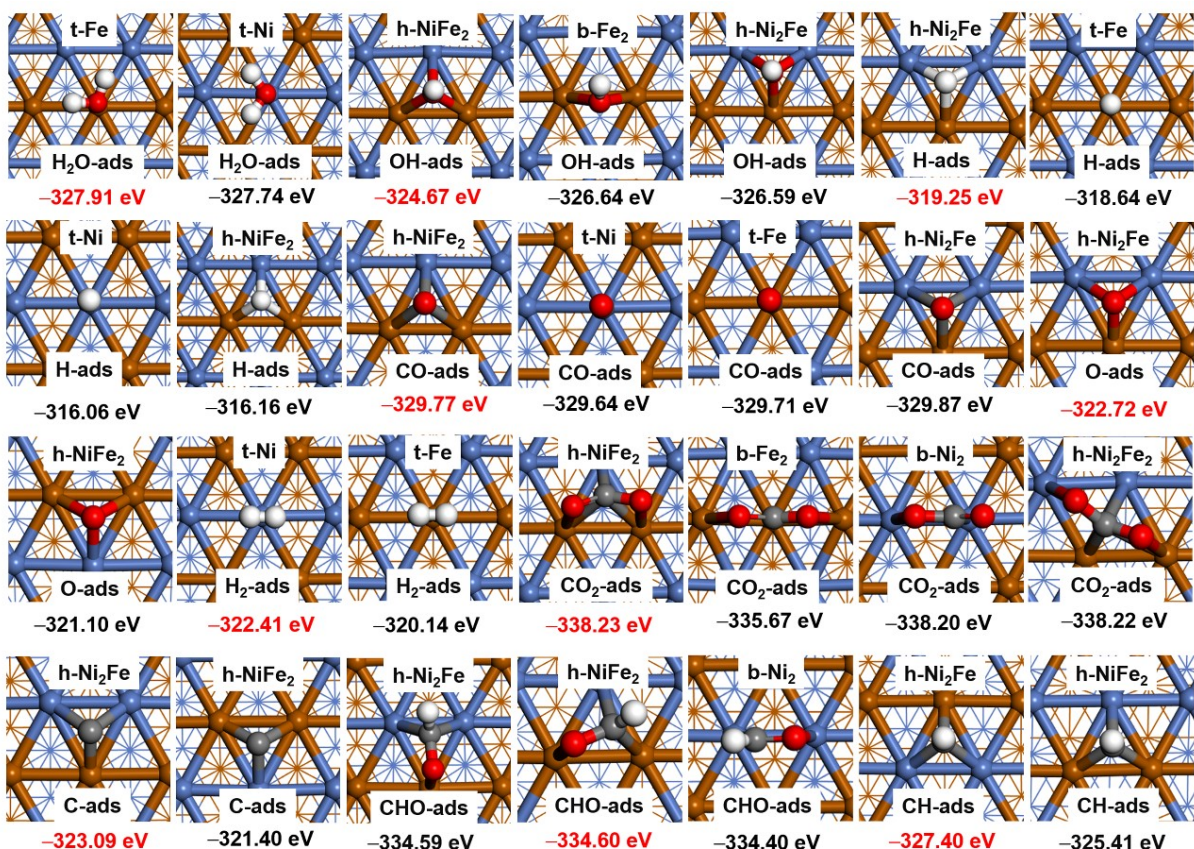


Fig. S7 Summary of the possible adsorption structures of H_2O , OH, H, CO, CHO, CH and C (including t-Fe, t-Ni, b-NiFe, b-Ni₂, b-Fe₂, h-Ni₂Fe, h-NiFe₂ sites) on NiFe (111) surface.

The most stable adsorption structures of H_2O , OH, H, CO, O, C, CH, COOH, CHO and HCOO

are the t-Co site, h-NiCo₂ site, h-NiCo₂ site, h-Ni₂Co site, h-NiCo₂ site, h-NiCo₂ site, h-Ni₂Co site, b-Co₂ site, b-Co₂ site and b-Co₂ site on the NiCo(111) surface, respectively, as highlighted in red in **Fig. S8**.

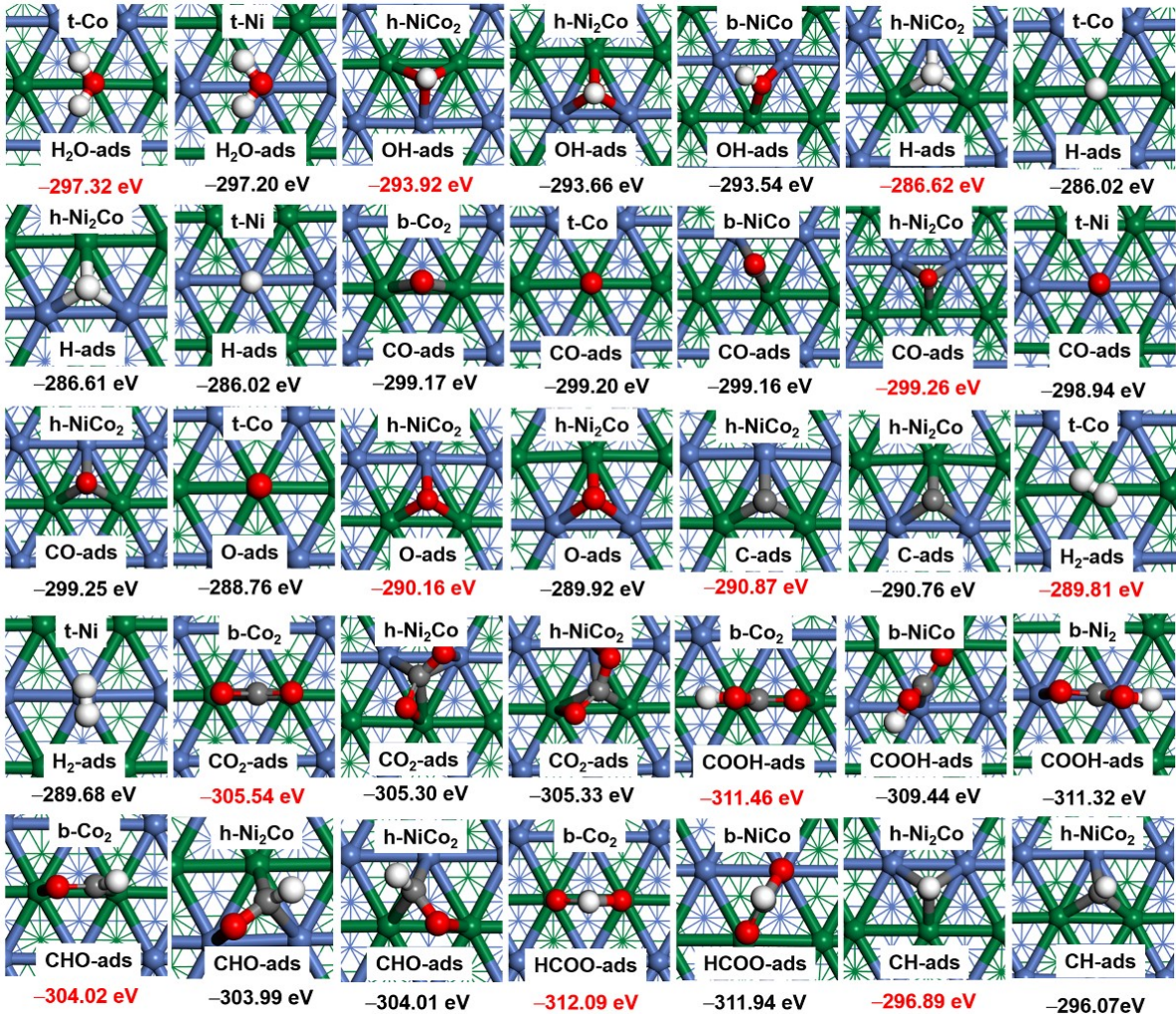


Fig. S8 Summary of the possible adsorption structures of H₂O, OH, H, O, CO, CO₂, CHO, CH, COOH, CHO and HCOO sites (including t-Co, t-Ni, b-NiCo, b-Ni₂, b-Co₂, h-Ni₂Co, h-NiCo₂ sites) on NiCo(111) surface.

The most stable adsorption structures of H₂O, OH, H, O, H₂, CO, CO₂, CHO, CH, and C are t-Ni site, h-NiCu₂, h-NiCu₂, h-NiCu₂, t-Ni site, b-Ni₂ site, t-Ni site, b-Ni₂ site, h-NiCu₂, and h-NiCu₂ site on the NiCu(111) surface, respectively, as highlighted in red in **Fig. S9**.

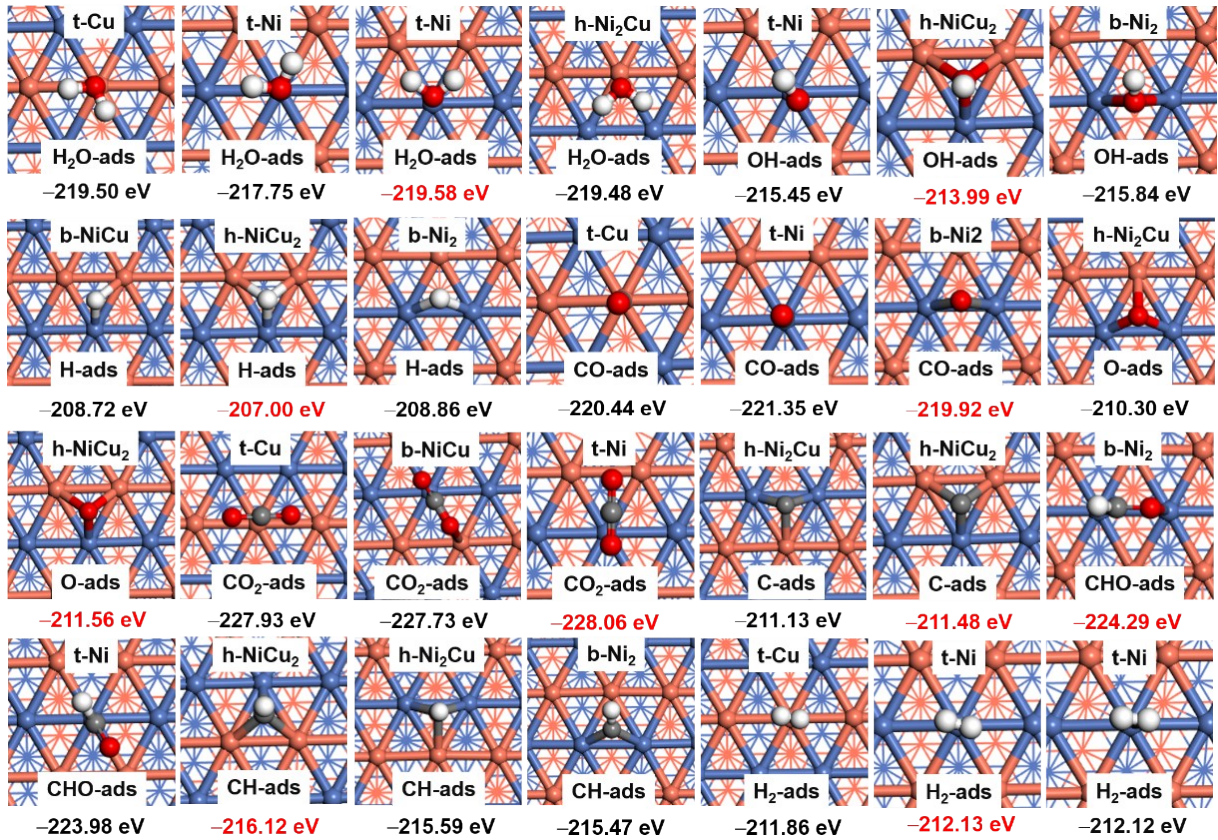


Fig. S9 Summary of the possible adsorption structures of H_2O , H_2 , OH , O , H , CO , CO_2 , CHO , CH and C sites (including t-Cu, t-Ni, b-NiCu, b-Ni₂, b-Cu₂, h-Ni₂Cu, h-NiCu₂ sites) on NiCu(111) surfaces.

H_2O , OH , H , CO , CHO , CH , C and CO_2 are most stably bonded with the t-Ni site, h-Ni₂Zn site, b-Ni₂ site, b-NiZn site, b-Ni₂Zn₂, h-Ni₂Zn on the NiZn (111) surface, respectively, as highlighted in red in **Fig. S10**.

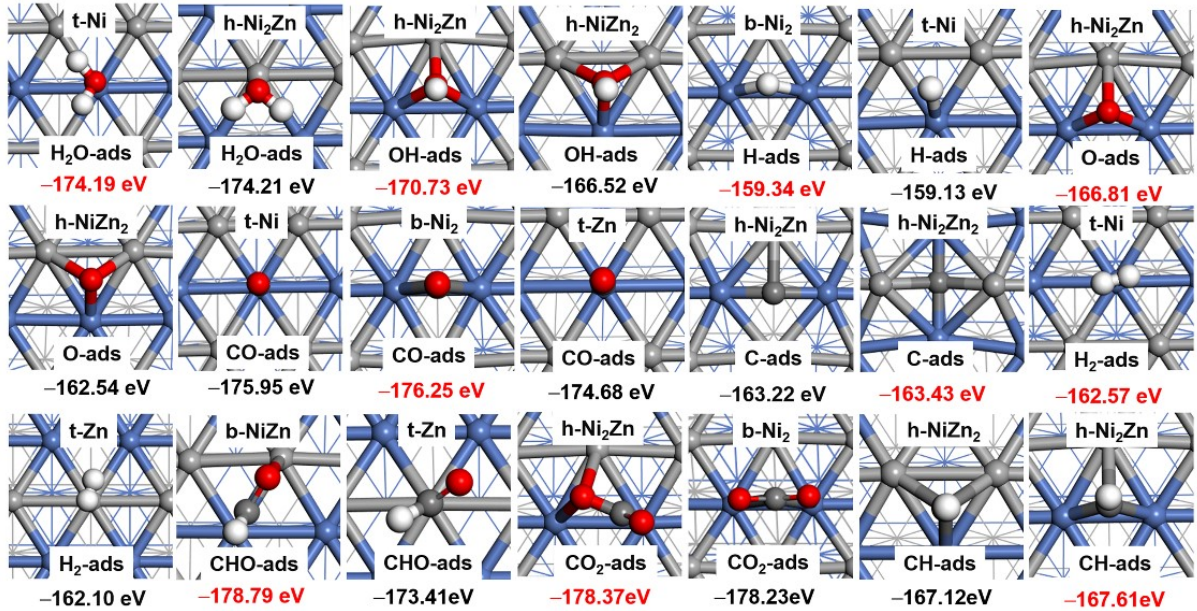


Fig. S10 Summary of the possible adsorption structures of H₂O, OH, H, CO, CHO, CH, C, CO₂ sites (including t-Zn, t-Ni, b-NiZn, b-Ni₂, b-Zn₂, h-Ni₂Zn, h-NiZn₂ sites) on NiZn(111) surface.

5. The size and the average charge of adsorption sites

The factors affecting the adsorption energy of species includes two types: the size factor (strain effect) and the electron factor (ligand effect). The size factor (r) is equal to the sum of the atomic radius that make up the site (t-Ni: $r = R_{\text{Ni}}$; t-M: $r = R_M$; b-Ni₂: $r = 2R_{\text{Ni}}$; b-NiM: $r = R_{\text{Ni}} + R_M$; b-M₂: $r = 2R_M$; h-Ni₃: $r = 3R_{\text{Ni}}$; h-Ni₂M: $r = 2R_{\text{Ni}} + R_M$; h-NiM₂: $r = R_{\text{Ni}} + 2R_M$, **Table S10, Fig. S11**). The calculation results of the sizes of adsorption sites of H₂O*, CO*, H₂* and CO₂* are shown in **Fig. S13**. It can be obtained that the size of these sites ($R_{\text{Fe}} > R_{\text{Ni}}$; $R_{\text{Co}} > R_{\text{Ni}}$) on the NiFe(111) and NiCo(111) surfaces are larger than that of pure Ni(111), which are expansive strain. While NiCu(111) and NiZn(111) surfaces are lower than that of pure Ni(111) ($R_{\text{Cu}} < R_{\text{Ni}}$; $R_{\text{Zn}} < R_{\text{Ni}}$), which are compressive strain.

While analyzing the electron factor, it can be found that the electron factor represents the effects of the atomic nuclei on the outer shell and the valence electrons, as well as the interactions between the outer and valence electrons and between the ions themselves, which is similar to the ligand effect.

Here note that the $q_M > q_{Ni}$ ($q_M < q_{Ni}$) indicates negatively (positively) charged NiM surface compared pure Ni(111). The electron factor (λ) is equal to the average valence electron at the site (t-Ni: $\lambda = q_{Ni}$; t-M: $\lambda = q_M$; b-Ni₂: $\lambda = (q_{Ni} + q_{Ni})/2$; b-NiM: $\lambda = (q_{Ni} + q_M)/2$; b-M₂: $\lambda = (q_M + q_M)/2$; h-Ni₃: $\lambda = (q_{Ni} + q_{Ni})/3$; h-Ni₂M: $\lambda = (2q_{Ni} + q_M)/3$; h-NiM₂: $\lambda = (q_{Ni} + 2q_M)/3$, **Table S10** and **Fig. S12**). The calculation results of the average charge of adsorption sites of H₂O*, CO*, H₂* and CO₂* are shown in **Fig. S13**. It is found that the charge of these sites on the NiFe(111) and NiCo(111) surfaces ($q_{Fe} < q_{Ni}$; $q_{Co} < q_{Ni}$) are lower than that of pure Ni(111) ($\leq 10.0|e|$), which are positively charged. And NiCu(111) and NiZn (111) surfaces ($q_{Cu} > q_{Ni}$; $q_{Zn} > q_{Ni}$) are higher than that of pure Ni(111) ($\geq 10.0|e|$), which are negatively charged.

Table S10. The size (r , in Å) and the average charge (λ , in |e|) of adsorption sites involved on Ni(111) and NiM(111) surfaces

Adsorption Site	$\lambda/ e $	$r/\text{\AA}$	Adsorption Site	$\lambda/ e $	$r/\text{\AA}$
t-Ni	10	1.49	b-NiCu	10.53	2.94
t-Ni(Fe)	10.22	1.49	b-NiZn	11.02	2.91
t-Ni(Co)	10.1	1.49	b-Fe ₂	7.82	3.12
t-Ni(Cu)	10.08	1.49	b-Co ₂	8.95	3.04
t-Ni(Zn)	10.2	1.49	b-Cu ₂	10.97	2.90
t-Fe	7.82	1.56	b-Zn ₂	11.84	2.84
t-Co	8.95	1.52	h-Ni ₃	10	4.47
t-Cu	10.97	1.45	h-Ni ₂ Fe	9.42	4.54
t-Zn	11.84	1.42	h-NiFe ₂	8.62	4.61

b-Ni ₂	10	2.98	—	h-Ni ₂ Co	9.72	4.50
b-Ni ₂ (Fe)	10.22	2.98	—	h-NiCo ₂	9.34	4.53
b-Ni ₂ (Co)	10.1	2.98	—	h-Ni ₂ Cu	10.39	4.43
b-Ni ₂ (Cu)	10.08	2.98	—	h-NiCu ₂	10.67	4.39
b-Ni ₂ (Zn)	10.2	2.98	—	h-Ni ₂ Zn	10.75	4.40
b-NiFe	9.02	3.05	—	h-NiZn ₂	11.29	4.33
b-NiCo	9.53	3.01	—			

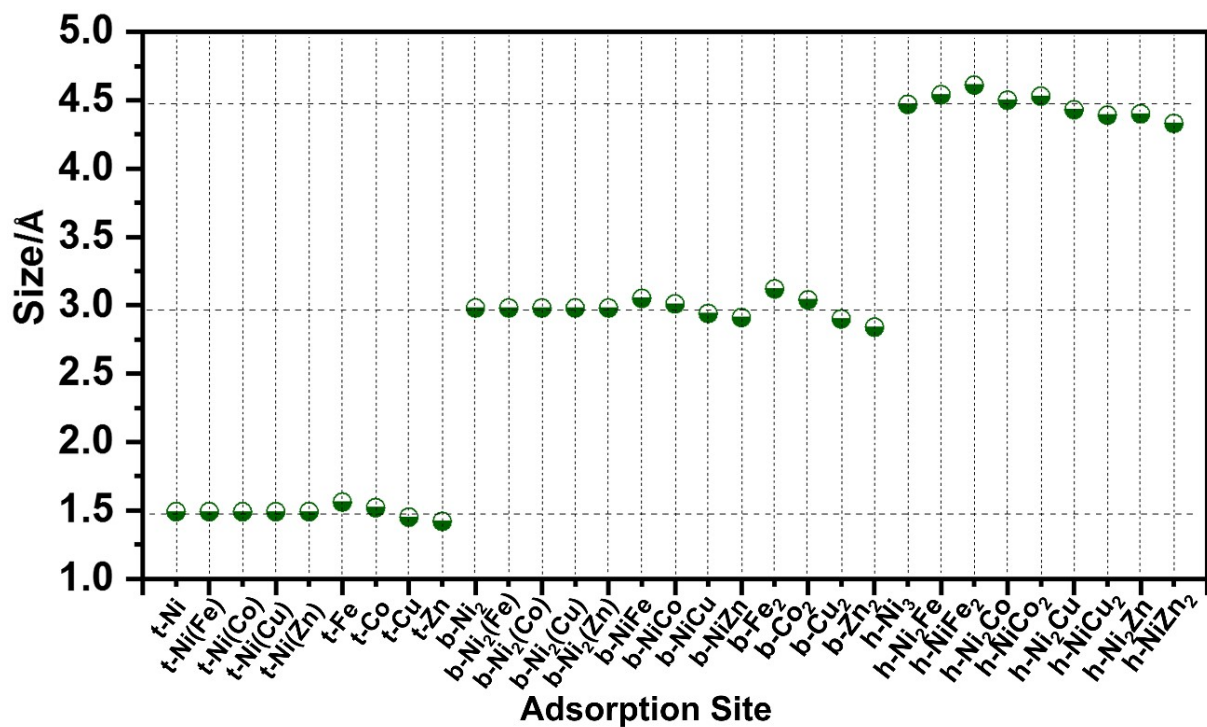


Fig. S11. The adsorption sites as a function of adsorption site size (r) on the Ni(111), NiFe(111), NiCo(111), NiCu(111) and NiZn(111) surfaces.

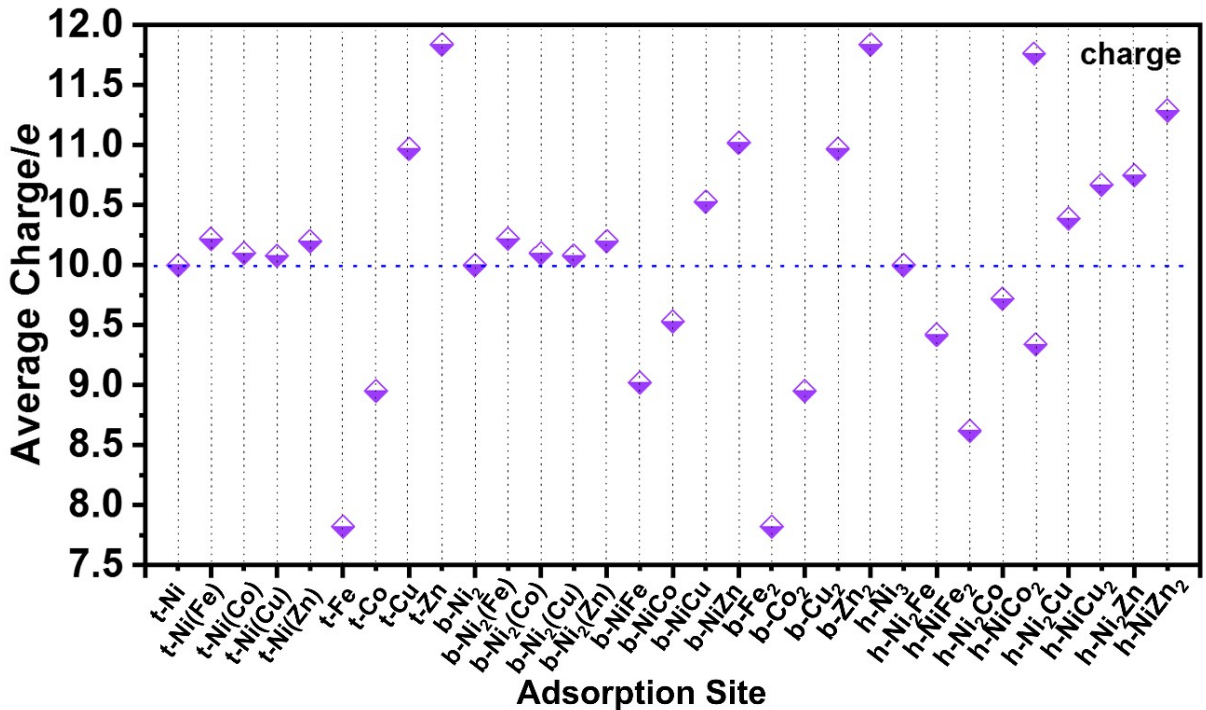


Fig. S12. The adsorption sites as a function of average charge (λ) of adsorption site on the Ni(111), NiFe(111), NiCo(111), NiCu(111) and NiZn(111) surfaces.

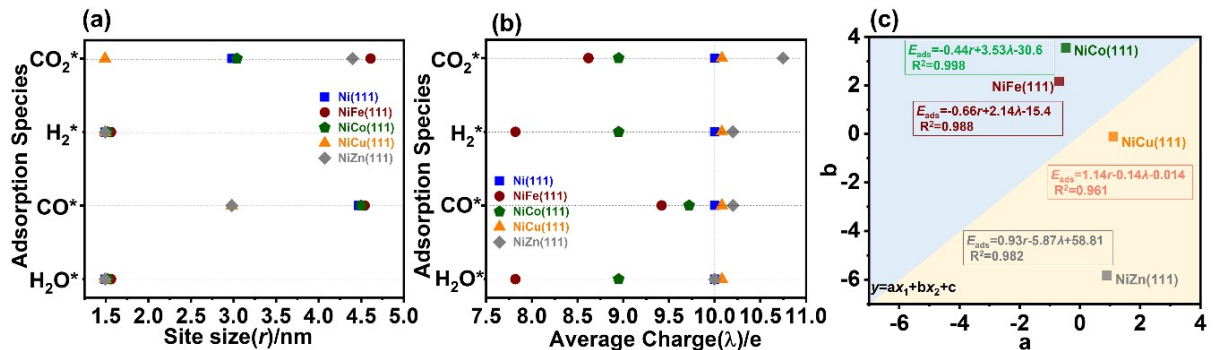


Fig. S13. (a) The adsorption sites of H₂O*, CO*, H₂* and CO₂* as a function of adsorption site size (r); and (b) average charge (λ) of adsorption site on the Ni(111), NiFe(111), NiCo(111), NiCu(111) and NiZn(111) surfaces; (c) The adsorption energies of H₂O*, CO*, H₂* and CO₂* as a function of radius and average charge of adsorption site on the NiFe(111), NiCo(111), NiCu(111) and NiZn(111) surfaces. Here “a” and “b” refer to the influence factors of the size (strain) (r) and the charge (λ) on the adsorption energy (E_{ads}), respectively.

6. Adsorption of H₂O and CO on Fe(110), Co(111), Cu(111) and Zn(001) surfaces

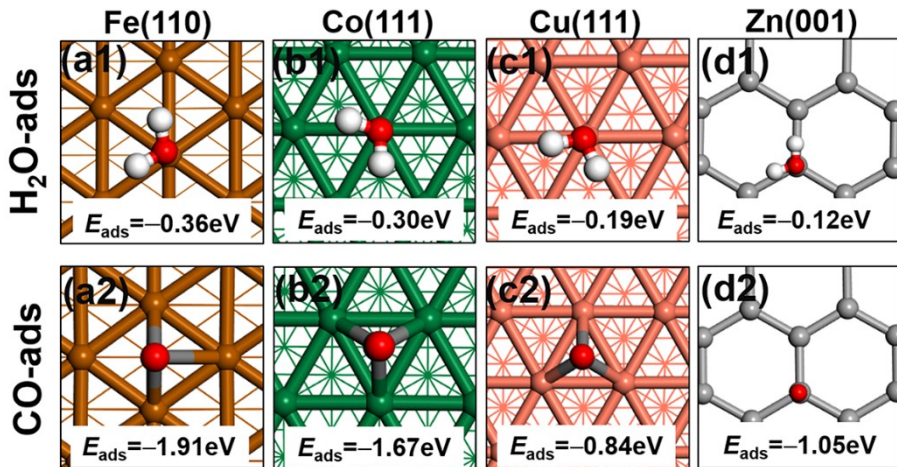


Fig. S14. The top view of the optimized structures of H_2O and CO adsorption on (a) $\text{Fe}(110)$, (b) $\text{Co}(111)$, (c) $\text{Cu}(111)$ and (d) $\text{Zn}(001)$ surfaces, along with the adsorption energies (E_{ads}). (Fe: maroon; Co: green; Cu: light brown; Zn: grey; O: red; H: white; C: dark gray).

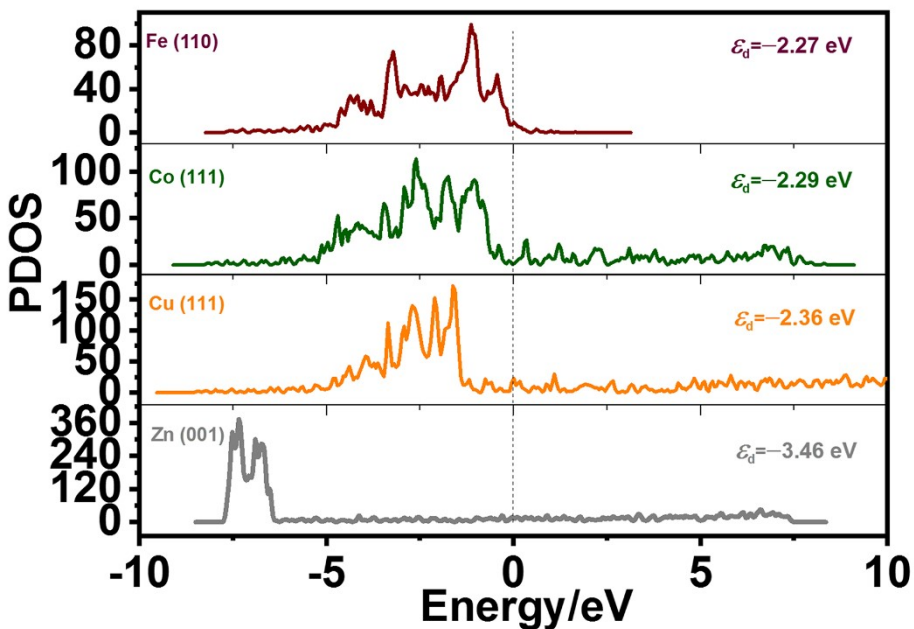


Fig. S15. The values of d -band center of $\text{Fe}(110)$, $\text{Co}(111)$, $\text{Cu}(111)$, $\text{Zn}(001)$ surfaces

Table S11. Total Energies (E) and total Energies with entropy effect correction (E_{entropy}) of the reaction intermediates on NiFe(111), NiCo(111), NiCu (111) and NiZn(111) surfaces

	$\text{CO}^*\rightleftharpoons\text{C}^* + \text{O}^*$	E/eV	$E_{\text{entropy}}/\text{eV}$
NiFe(111)	CO*	-329.77	-329.79
	TS	-326.71	-326.73
	C^*+O^*	-329.11	-329.14
NiCo(001)	$\text{CHO}^*\rightleftharpoons\text{CH}^* + \text{O}^*$	E/eV	$E_{\text{entropy}}/\text{eV}$
	CHO*	-332.60	-332.63
	TS	-331.16	-331.18
NiCu(111)	CH^*+O^*	-333.25	-333.26
	$\text{CO}^*+\text{CO}^*\rightleftharpoons\text{CO}_2^* + \text{C}^*$	E/eV	$E_{\text{entropy}}/\text{eV}$
	CO*+CO*	-346.12	-346.13
NiZn(111)	TS	-340.02	-340.03
	$\text{CO}_2^* + \text{C}^*$	-344.42	-344.44
	$\text{H}_2\text{O}^* + \cdot \rightleftharpoons \text{OH}^* + \text{H}^*$	E/eV	$E_{\text{entropy}}/\text{eV}$
NiFe(111)	H ₂ O*	-327.91	-327.93
	TS	-326.70	-326.72
	OH* + H*	-328.58	-328.60
NiCo(001)	$\text{CO}^*\rightleftharpoons\text{C}^* + \text{O}^*$	E/eV	$E_{\text{entropy}}/\text{eV}$
	CO*	-299.26	-299.28
	TS	-296.42	-296.44
NiCu(111)	$\text{C}^* + \text{O}^*$	-298.11	-298.15
	$\text{CHO}^*\rightarrow\text{CH}^* + \text{O}^*$	E/eV	$E_{\text{entropy}}/\text{eV}$
	CHO*	-301.99	-302.02
NiZn(111)	TS	-300.33	-300.35
	$\text{CH}^* + \text{O}^*$	-302.57	-302.60
	$\text{CO}^*+\text{CO}^*\rightleftharpoons\text{CO}_2^* + \text{C}^*$	E/eV	$E_{\text{entropy}}/\text{eV}$
NiFe(111)	CO*+CO*	-315.71	-315.73
	TS	-311.45	-311.47
	$\text{CO}_2^* + \text{C}^*$	-315.78	-315.79
NiCo(001)	$\text{H}_2\text{O}^* \rightleftharpoons \text{OH}^* + \text{H}^*$	E/eV	$E_{\text{entropy}}/\text{eV}$
	H ₂ O*	-297.32	-297.34
	TS	-296.72	-296.74
NiCu(111)	OH*+H*	-297.65	-297.67
	$\text{CO}^*\rightleftharpoons\text{C}^* + \text{O}^*$	E/eV	$E_{\text{entropy}}/\text{eV}$
	CO*	-219.92	-219.94
NiZn(111)	TS	-216.67	-216.69
	$\text{C}^* + \text{O}^*$	-217.96	-217.98
	$\text{CHO}^*\rightleftharpoons\text{CH}^* + \text{O}^*$	E/eV	$E_{\text{entropy}}/\text{eV}$
NiFe(111)	CHO*	-222.55	-222.58
	TS	-220.70	-220.72
	$\text{CH}^* + \text{O}^*$	-222.47	-222.49
NiCo(001)	$\text{CO}^*+\text{CO}^*\rightleftharpoons\text{CO}_2^* + \text{O}^*$	E/eV	$E_{\text{entropy}}/\text{eV}$

NiZn(111)	CO*+CO*	-236.52	-236.54
	TS	-232.10	-232.12
	CO ₂ *+ O*	-235.26	-235.28
	H ₂ O* ⇌ OH*+H*	<i>E/eV</i>	<i>E_{entropy}/eV</i>
	H ₂ O*	-217.75	-217.77
	TS	-216.72	-216.74
	OH*+H*	-217.50	-217.52
	CO* ⇌ C* + O*	<i>E/eV</i>	<i>E_{entropy}/eV</i>
	CO*	-176.25	-176.27
	TS	-173.17	-173.19
	C* + O*	-173.98	-174.01
	CHO* ⇌ CH*+ O*	<i>E/eV</i>	<i>E_{entropy}/eV</i>
	CHO*	-178.79	-178.81
	TS	-177.27	-177.29
	CH*+ O*	-178.53	-178.55
	CO*+CO* ⇌ CO ₂ *+ O*	<i>E/eV</i>	<i>E_{entropy}/eV</i>
	CO*+CO*	-192.47	-192.49
	TS	-188.44	-188.46
	CO ₂ *+ O*	-189.74	-189.76
	H ₂ O* ⇌ OH*+H*	<i>E/eV</i>	<i>E_{entropy}/eV</i>
	H ₂ O*	-174.23	-174.25
	TS	-172.98	-173.00
	OH*+H*	-174.64	-174.66

7. WGSR elementary reaction step on NiCo(111) and NiCu(111) surfaces

7.1. Adsorption structures and adsorption energies

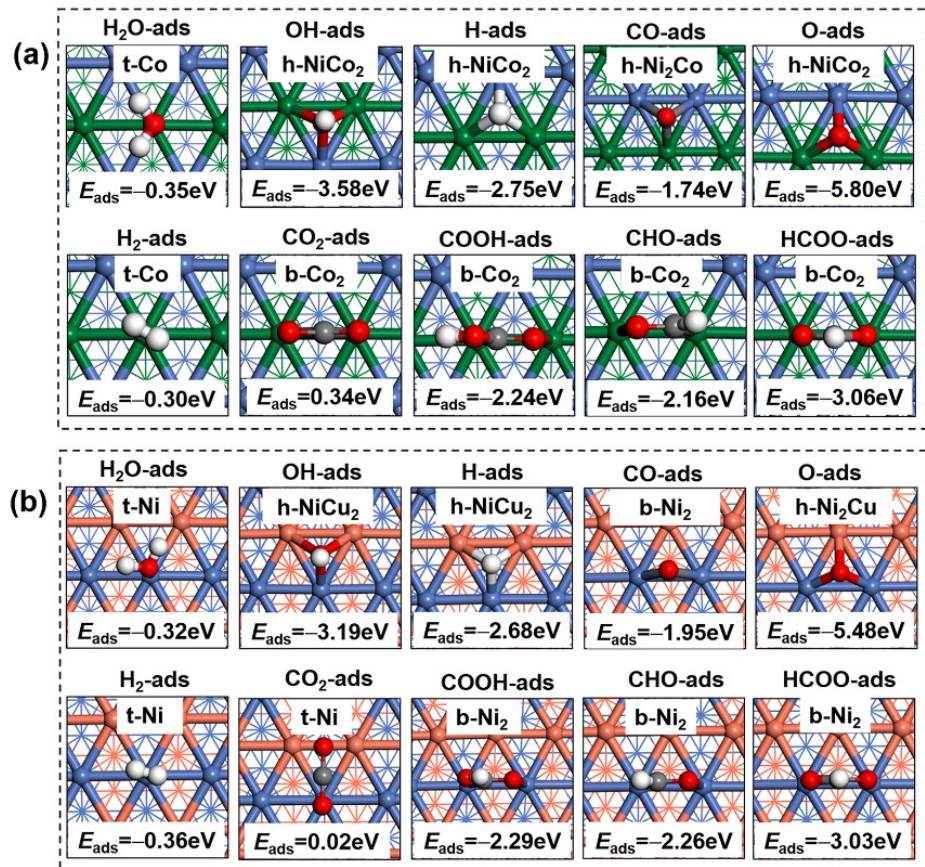


Fig. S16. Adsorption structures and adsorption energies of H₂O, H₂, OH, O, H, CO, CO₂, COOH, CHO and HCOO on NiCo(111) (a) and NiCu(111) (b) surfaces.

7.2 Structures of reactants, transition states and products

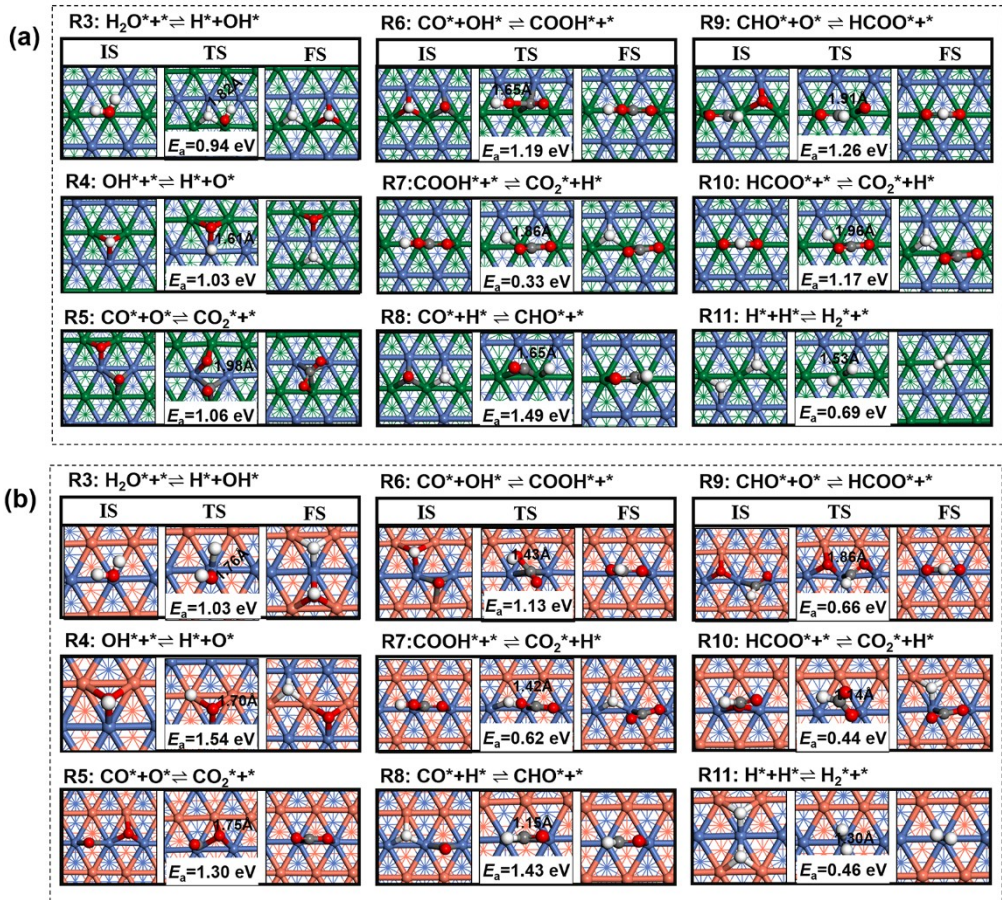


Fig. S17. Initial state(IS), the corresponding transition state(TS) and final state(FS) structures and energies barrier(E_a) of WGSR element steps on the NiCo(111) (a) and NiCu(111) (b) surfaces.

Table S12. The Total Energies (E), total Energies with entropy effect correction (E_{entropy}) of the reaction intermediates on the NiCo(111) and NiCu(111) surfaces

		NiCo(111)		NiCu(111)	
$\text{H}_2\text{O}^* + * \rightleftharpoons \text{OH}^* + \text{H}^*$	E/eV	$E_{\text{entropy}}/\text{eV}$	E/eV	$E_{\text{entropy}}/\text{eV}$	
H_2O^*	-297.32	-297.34	-217.75	-217.77	
TS3	-296.38	-296.40	-216.72	-216.74	
$\text{OH}^* + \text{H}^*$	-297.65	-297.67	-217.50	-217.52	
$\text{OH}^* \rightleftharpoons \text{O}^* + \text{H}^*$	E/eV	$E_{\text{entropy}}/\text{eV}$	E/eV	$E_{\text{entropy}}/\text{eV}$	
OH^*	-293.92	-293.94	-213.99	-214.01	
TS4	-292.77	-292.79	-212.26	-212.28	
$\text{O}^* + \text{H}^*$	-294.05	-294.07	-213.59	-214.61	
$\text{CO}^* + \text{O}^* \rightarrow \text{CO}_2^*$	E/eV	$E_{\text{entropy}}/\text{eV}$	E/eV	$E_{\text{entropy}}/\text{eV}$	
$\text{CO}^* + \text{O}^*$	-306.53	-306.55	-226.79	-226.81	
TS5	-305.46	-305.48	-225.46	-225.48	
CO_2^*	-305.60	-305.62	-226.12	-226.14	
$\text{CO}^* + \text{OH}^* \rightleftharpoons \text{COOH}^*$	E/eV	$E_{\text{entropy}}/\text{eV}$	E/eV	$E_{\text{entropy}}/\text{eV}$	

$\text{CO}^* + \text{OH}^*$	-310.27	-310.29	-230.34	-230.36
TS6	-309.08	-309.10	-229.21	-229.23
COOH^*	-309.44	-309.46	-229.94	-229.96
$\text{COOH}^* \rightarrow \text{CO}_2^* + \text{H}^*$	E/eV	$E_{\text{entropy}}/\text{eV}$	E/eV	$E_{\text{entropy}}/\text{eV}$
COOH*	-309.44	-309.46	-230.01	-230.03
TS7	-308.87	-308.89	-229.16	-229.18
$\text{CO}_2^* + \text{H}^*$	-309.26	-309.28	-229.93	-229.95
$\text{CO}^* + \text{H}^* \rightleftharpoons \text{CHO}^*$	E/eV	$E_{\text{entropy}}/\text{eV}$	E/eV	$E_{\text{entropy}}/\text{eV}$
CO* + H*	-303.09	-303.11	-223.87	-223.89
TS8	-301.82	-301.84	-222.47	-222.49
CHO*	-301.99	-302.01	-222.55	-222.57
$\text{CHO}^* + \text{O}^* \rightleftharpoons \text{HCOO}^*$	E/eV	$E_{\text{entropy}}/\text{eV}$	E/eV	$E_{\text{entropy}}/\text{eV}$
CHO* + O*	-309.20	-309.22	-229.37	-229.39
TS9	-307.96	-307.98	-228.71	-228.73
HCOO*	-309.86	-309.88	-230.28	-230.30
$\text{HCOO}^* \rightarrow \text{CO}_2^* + \text{H}^*$	E/eV	$E_{\text{entropy}}/\text{eV}$	E/eV	$E_{\text{entropy}}/\text{eV}$
HCOO*	-309.86	-309.88	-229.72	-229.74
TS10	-308.59	-308.61	-229.23	-229.25
$\text{CO}_2^* + \text{H}^*$	-309.26	-309.28	-229.75	-229.77
$\text{H}^* + \text{H}^* \rightarrow \text{H}_2^*$	E/eV	$E_{\text{entropy}}/\text{eV}$	E/eV	$E_{\text{entropy}}/\text{eV}$
$\text{H}^* + \text{H}^*$	-290.52	-290.54	-210.74	-210.76
TS11	-289.77	-289.79	-210.19	-210.21
H_2^*	-289.92	-289.94	-210.33	-210.35

8. Microkinetic modeling analysis of WGS reaction

On the basis of DFT calculated results, a microkinetic modeling of WGS reaction over NiCo(111) and NiCu(111) surfaces are carried out. The **Table S13 and S14** list the elementary steps of WGS reaction over NiCo (111) and NiCu(111) surface. k_i is the rate constant (in s^{-1}), p is the pressure (in Pa), θ represents the coverage of the adsorbed species (in ML), θ^* represents the coverage of vacancies site. r_i is the rate of the elementary reaction step i (in $\text{s}^{-1} \cdot \text{site}^{-1}$). Since the adsorption of CO_2 and H_2 is very weak (**Fig. 2**), we assume that the product is immediately desorbed at the same time as the product is formed, so the step involving product formation (R5, R7, R10, R11) is a one-way reaction. Based on the reactions (1)-(11) rate equations as below, the equilibrium coverages(θ) of all species are solved

by Fortran program, as listed in the **Table S21-S22**.

$$(1) \frac{d\theta_{CO^*}}{dt} = k_1 p_{CO}/p^\Theta \theta^* - k_{-1} \theta_{CO^*} - k_5 \theta_{CO^*} \theta_{O^*} - k_6 \theta_{OH^*} \theta_{CO^*} + k_{-6} \theta_{COOH^*} \theta^* - k_8 \theta_{H^*} \theta_{CO^*} + k_{-8} \theta_{HCO^*} \theta^*$$

$$= r_1 - r_5 - r_6 - r_8$$

$$(2) \frac{d\theta_{H_2O^*}}{dt} = k_2 p_{H_2O(g)}/p^\Theta \theta^* - k_{-2} \theta_{H_2O^*} - k_3 \theta_{H_2O^*} \theta^* + k_{-3} \theta_{OH^*} \theta_{H^*} = r_2 - r_3$$

$$(3) \frac{d\theta_{OH^*}}{dt} = k_3 \theta_{H_2O^*} \theta^* - k_{-3} \theta_{OH^*} \theta_{H^*} - k_4 \theta_{OH^*} \theta^* + k_{-4} \theta_{H^*} \theta_{O^*} - k_6 \theta_{OH^*} \theta_{CO^*} + k_{-6} \theta_{COOH^*} \theta^* = r_3 - r_4 - r_6$$

$$(4) \frac{d\theta_{H^*}}{dt} = k_3 \theta_{H_2O^*} \theta^* - k_{-3} \theta_{OH^*} \theta_{H^*} + k_4 \theta_{OH^*} \theta^* - k_{-4} \theta_{H^*} \theta_{O^*} + k_7 \theta_{COOH^*} \theta^* - k_8 \theta_{H^*} \theta_{CO^*} + k_{-8} \theta_{CHO^*} \theta^* +$$

$$k_{10} \theta_{HCOO^*} \theta^* - k_{11} \theta_{H^*} \theta_{H^*} = r_3 + r_4 + r_7 - r_8 + r_{10} - r_{11}$$

$$(5) \frac{d\theta_{O^*}}{dt} = k_4 \theta_{OH^*} \theta^* - k_{-4} \theta_{H^*} \theta_{O^*} - k_5 \theta_{CO^*} \theta_{O^*} - k_9 \theta_{CHO^*} \theta_{O^*} + k_{-9} \theta_{HCOO^*} \theta^* = r_4 - r_5 - r_9$$

$$(6) \frac{d\theta_{COOH^*}}{dt} = k_6 \theta_{OH^*} \theta_{CO^*} - k_{-6} \theta_{COOH^*} \theta^* - k_7 \theta_{COOH^*} \theta^* = r_6 - r_7$$

$$(7) \frac{d\theta_{CHO^*}}{dt} = k_8 \theta_{H^*} \theta_{CO^*} - k_{-8} \theta_{CHO^*} \theta^* - k_9 \theta_{CHO^*} \theta_{O^*} + k_{-9} \theta_{HCOO^*} \theta^* = r_8 - r_9$$

$$(8) \frac{d\theta_{HCOO^*}}{dt} = k_9 \theta_{CHO^*} \theta_{O^*} - k_{-9} \theta_{HCOO^*} \theta^* - k_{10} \theta_{HCOO^*} \theta^* = r_9 - r_{10}$$

$$(9) \frac{d\theta_{CO_2^*}}{dt} = k_5 \theta_{CO^*} \theta_{O^*} + k_7 \theta_{COOH^*} \theta^* + k_{10} \theta_{HCOO^*} \theta^* = r_5 + r_7 + r_{10}$$

$$(10) \frac{d\theta_{H_2^*}}{dt} = k_{11} \theta_{H^*} \theta_{H^*} = r_{11}$$

$$(11) \frac{d\theta_*}{dt} = -k_1 p_{CO}/p^\Theta \theta^* + k_{-1} \theta_{CO^*} - k_2 p_{H_2O(g)}/p^\Theta \theta^* + k_{-2} \theta_{H_2O^*} - k_3 \theta_{H_2O^*} \theta^* + k_{-3} \theta_{OH^*} \theta_{H^*} - k_4 \theta_{OH^*} \theta^* + k_{-4} \theta_{H^*} \theta_{O^*} +$$

$$k_5 \theta_{CO^*} \theta_{O^*} + k_6 \theta_{OH^*} \theta_{CO^*} - k_{-6} \theta_{COOH^*} \theta^* - k_7 \theta_{COOH^*} \theta^* + k_8 \theta_{H^*} \theta_{CO^*} - k_{-8} \theta_{CHO^*} \theta^* + k_9 \theta_{CHO^*} \theta_{O^*} - k_{-9} \theta_{HCOO^*} \theta^* -$$

$$k_{10} \theta_{HCOO^*} \theta^* + k_{11} \theta_{H^*} \theta_{H^*} = -r_1 - r_2 - r_3 - r_4 + r_5 + r_6 - r_7 + r_8 + r_9 - r_{10} + r_{11}$$

Table S13. Rate equations and the calculated pre-exponential factors (v , in s^{-1}) of each elementary step of WGS reaction over NiCo(111) surface

reaction steps	rate equations	v_{for}/s^{-1}	v_{rev}/s^{-1}
R1 CO + * ⇌ CO *	$r_1 = k_1 p_{CO}/p^\Theta \theta^* - k_{-1} \theta_{CO^*}$	-	-

R2	$\text{H}_2\text{O}(g) + * \rightleftharpoons \text{H}_2\text{O}^*$	$r_2 = k_2 p_{\text{H}_2\text{O}(g)} / p^\Theta \theta^* - k_{-2} \theta_{\text{H}_2\text{O}^*}$	—	—
R3	$\text{H}_2\text{O}^* + * \rightleftharpoons \text{OH}^* + \text{H}^*$	$r_3 = k_3 \theta_{\text{H}_2\text{O}^*} \theta^* - k_{-3} \theta_{\text{OH}^*} \theta_{\text{H}^*}$	7.67×10^{12}	2.30×10^{14}
R4	$\text{OH}^* + * \rightleftharpoons \text{H}^* + \text{O}^*$	$r_4 = k_4 \theta_{\text{OH}^*} \theta^* - k_{-4} \theta_{\text{H}^*} \theta_{\text{O}^*}$	1.02×10^{12}	1.90×10^{14}
R5	$\text{CO}^* + \text{O}^* \rightarrow \text{CO}_2^* + *$	$r_5 = k_5 \theta_{\text{CO}^*} \theta_{\text{O}^*}$	1.44×10^{13}	2.35×10^{12}
R6	$\text{CO}^* + \text{OH}^* \rightleftharpoons \text{COOH}^* + *$	$r_6 = k_6 \theta_{\text{OH}^*} \theta_{\text{CO}^*} - k_{-6} \theta_{\text{COOH}^*} \theta^*$	2.96×10^{14}	1.15×10^{15}
R7	$\text{COOH}^* + * \rightarrow \text{H}^* + \text{CO}_2^*$	$r_7 = k_7 \theta_{\text{COOH}^*} \theta^*$	1.42×10^{15}	1.84×10^{14}
R8	$\text{CO}^* + \text{H}^* \rightleftharpoons \text{CHO}^* + *$	$r_8 = k_8 \theta_{\text{H}^*} \theta_{\text{CO}^*} - k_{-8} \theta_{\text{HCO}^*} \theta^*$	3.62×10^{12}	1.64×10^{13}
R9	$\text{CHO}^* + \text{O}^* \leftrightarrow \text{HCOO}^* + *$	$r_9 = k_9 \theta_{\text{HCO}^*} \theta_{\text{O}^*} - k_{-9} \theta_{\text{HCOO}^*} \theta^*$	5.42×10^{13}	1.05×10^{14}
R10	$\text{HCOO}^* + * \rightarrow \text{H}^* + \text{CO}_2^*$	$r_{10} = k_{10} \theta_{\text{HCOO}^*} \theta^*$	1.30×10^{14}	8.78×10^{12}
R11	$2\text{H}^* \rightarrow \text{H}_2^* + *$	$r_{11} = k_{11} \theta_{\text{H}^*} \theta_{\text{H}^*}$	4.63×10^{15}	3.90×10^{14}

Table S14. Rate equations and the calculated pre-exponential factors (v , in s^{-1}) of each elementary step of WGS reaction over NiCu(111) surface

reaction steps	rate equations	$v_{\text{for}}/\text{s}^{-1}$	$v_{\text{rev}}/\text{s}^{-1}$
R1	$\text{CO} + * \rightleftharpoons \text{CO}^*$	$r_1 = k_1 p_{\text{CO}} / p^\Theta \theta^* - k_{-1} \theta_{\text{CO}^*}$	—
R2	$\text{H}_2\text{O}(g) + * \rightleftharpoons \text{H}_2\text{O}^*$	$r_2 = k_2 p_{\text{H}_2\text{O}(g)} / p^\Theta \theta^* - k_{-2} \theta_{\text{H}_2\text{O}^*}$	—
R3	$\text{H}_2\text{O}^* + * \rightleftharpoons \text{OH}^* + \text{H}^*$	$r_3 = k_3 \theta_{\text{H}_2\text{O}^*} \theta^* - k_{-3} \theta_{\text{OH}^*} \theta_{\text{H}^*}$	2.31×10^{12}
R4	$\text{OH}^* + * \rightleftharpoons \text{H}^* + \text{O}^*$	$r_4 = k_4 \theta_{\text{OH}^*} \theta^* - k_{-4} \theta_{\text{H}^*} \theta_{\text{O}^*}$	3.83×10^{13}
R5	$\text{CO}^* + \text{O}^* \rightarrow \text{CO}_2^* + *$	$r_5 = k_5 \theta_{\text{CO}^*} \theta_{\text{O}^*}$	1.77×10^{13}
R6	$\text{CO}^* + \text{OH}^* \rightleftharpoons \text{COOH}^* + *$	$r_6 = k_6 \theta_{\text{OH}^*} \theta_{\text{CO}^*} - k_{-6} \theta_{\text{COOH}^*} \theta^*$	2.65×10^{13}
R7	$\text{COOH}^* + * \rightarrow \text{H}^* + \text{CO}_2^*$	$r_7 = k_7 \theta_{\text{COOH}^*} \theta^*$	1.42×10^{14}
R8	$\text{CO}^* + \text{H}^* \rightleftharpoons \text{CHO}^* + *$	$r_8 = k_8 \theta_{\text{H}^*} \theta_{\text{CO}^*} - k_{-8} \theta_{\text{HCO}^*} \theta^*$	1.46×10^{13}
			5.82×10^{13}

R9	$\text{CHO}^* + \text{O}^* \leftrightarrow \text{HCOO}^* + *$	$r_9 = k_9 \theta_{\text{HCO}^*} \theta_{\text{O}^*} - k_{-9} \theta_{\text{HCOO}^*} \theta^*$	6.04×10^{12}	1.49×10^{13}
R10	$\text{HCOO}^* + * \rightarrow \text{H}^* + \text{CO}_2^*$	$r_{10} = k_{10} \theta_{\text{HCOO}^*} \theta^*$	8.46×10^{12}	3.10×10^{13}
R11	$2\text{H}^* \rightarrow \text{H}_2^* + *$	$r_{11} = k_{11} \theta_{\text{H}^*} \theta_{\text{H}^*}$	8.96×10^{14}	1.10×10^{14}

For the microkinetic modeling, the equilibrium constants (K) are calculated only for the first two steps of WGS reaction (CO and H₂O adsorption, R1, R2). In this work, for the adsorption equilibrium constant (*Eq. S4* $K = \exp[-(E_{\text{ads}} - T\Delta S)/k_B T]$), the standard entropy (S) of CO and H₂O (g) gas referred from NIST Chemistry Web Book which include the translational, rotational and vibrational entropy (**Table S15**). For solid, the translational and rotational entropies are significantly smaller than the vibration entropy, they can be neglected and are not included in calculation of entropy. Therefore, entropy of adsorbed species is obtained from the standard vibrational entropy (S_{vib}°) in *Eq.S8*,

$$S_{\text{vib}}^{\circ} = R \sum_i \left\{ \frac{hc\nu_i / k_B T}{e^{hc\nu_i / k_B T} - 1} - \ln \left(1 - e^{-hc\nu_i / k_B T} \right) \right\}.$$

Table S15. The entropy (S) data of CO and H₂O(g) from NIST Chemistry Web Book at 298.15 K

	Gas State	Gas State/eV
	$S_{\text{NIST}}/\text{kJ}\cdot\text{mol}^{-1}\cdot\text{K}^{-1}$	$TS_{\text{NIST}}/\text{eV}$
CO	197.66	0.60
H ₂ O	188.83	0.57

Table S16. Initial coverage of CO, H₂O and vacancies

θ_{CO^*}	$\theta_{\text{H}_2\text{O}^*}$	θ^*
0	0	1

Table S17. Equilibrium constant (K) of CO adsorption and H₂O adsorption steps on the NiCo(111) surface

K	$\text{CO} + * \leftrightarrow \text{CO}^*$	$\text{H}_2\text{O(g)} + * \leftrightarrow \text{H}_2\text{O}^*$
423.15	5.07×10^{20}	1.31×10^4
473.15	3.29×10^{18}	4.82×10^3
523.15	5.58×10^{16}	2.14×10^3
573.15	1.93×10^{15}	1.10×10^3
623.15	1.14×10^{14}	6.26×10^2
673.15	1.03×10^{13}	3.88×10^2
723.15	1.30×10^{12}	2.57×10^2

Table S18. Equilibrium constant (K) of CO adsorption and H₂O adsorption steps on the NiCu(111) surface

K	$\text{CO} + * \leftrightarrow \text{CO}^*$	$\text{H}_2\text{O(g)} + * \leftrightarrow \text{H}_2\text{O}^*$
423.15	1.57×10^{23}	7.41×10^3
473.15	5.53×10^{20}	2.89×10^3
523.15	5.75×10^{18}	1.35×10^3
573.15	1.33×10^{17}	7.20×10^2
623.15	5.60×10^{15}	4.24×10^2
673.15	3.79×10^{14}	2.71×10^2
723.15	3.72×10^{13}	1.84×10^2

Table S19. Reaction rate constant (k , in s^{-1}) of the elementary reaction step on NiCo(111) under different temperatures

	423K	473K	523K	573K	623K	673K	723K
k_1	7.14×10^7	6.75×10^7	6.42×10^7	6.13×10^7	5.88×10^7	5.66×10^7	5.46×10^7
k_{-1}	1.41×10^{-13}	2.05×10^{-11}	1.15×10^{-9}	3.18×10^{-8}	5.14×10^{-7}	5.48×10^{-6}	4.20×10^{-5}
k_2	2.41×10^8	2.28×10^8	2.17×10^8	2.07×10^8	1.98×10^8	1.91×10^8	1.84×10^8
k_{-2}	1.83×10^4	4.72×10^4	1.01×10^5	1.89×10^5	3.17×10^5	4.92×10^5	7.17×10^5
k_3	8.86×10^0	1.27×10^2	1.12×10^3	6.76×10^3	3.10×10^4	1.14×10^5	3.53×10^5
k_{-3}	1.06×10^{-1}	1.35×10^{-1}	1.70×10^{-1}	2.14×10^{-1}	2.68×10^{-1}	3.35×10^{-1}	4.19×10^{-1}
k_4	9.60×10^1	1.92×10^3	2.19×10^4	1.63×10^5	8.87×10^5	3.77×10^6	1.32×10^7
k_{-4}	1.36×10^0	1.76×10^0	2.26×10^0	2.89×10^0	3.66×10^0	4.62×10^0	5.82×10^0
k_5	8.21×10^0	1.79×10^2	2.15×10^3	1.68×10^4	9.43×10^4	4.09×10^5	1.45×10^6
k_6	2.47×10^1	7.54×10^2	1.20×10^4	1.18×10^5	8.03×10^5	4.12×10^6	1.69×10^7
k_{-6}	1.26×10^{13}	2.03×10^{13}	3.27×10^{13}	5.23×10^{13}	8.35×10^{13}	1.33×10^{14}	2.11×10^{14}
k_7	2.47×10^{12}	7.41×10^{12}	1.82×10^{13}	3.85×10^{13}	7.27×10^{13}	1.25×10^{14}	2.01×10^{14}
k_8	2.73×10^{-6}	1.86×10^{-4}	5.58×10^{-3}	9.17×10^{-2}	9.54×10^{-1}	6.97×10^0	3.85×10^1
k_{-8}	7.94×10^9	7.40×10^9	6.85×10^9	6.32×10^9	5.81×10^9	5.32×10^9	4.86×10^9
k_9	1.90×10^{-1}	7.36×10^0	1.41×10^2	1.62×10^3	1.25×10^4	7.14×10^4	3.20×10^5
k_{-9}	3.99×10^{-8}	5.10×10^{-8}	6.54×10^{-8}	8.39×10^{-8}	1.08×10^{-7}	1.37×10^{-7}	1.75×10^{-7}
k_{10}	3.80×10^1	1.22×10^2	2.03×10^3	2.09×10^4	1.48×10^5	7.83×10^5	3.30×10^6
k_{11}	5.20×10^9	4.22×10^{10}	2.26×10^{11}	8.93×10^{11}	2.81×10^{12}	7.39×10^{12}	1.70×10^{13}

Table S20. Reaction rate constant (k , in s^{-1}) of the elementary reaction step on NiCu(111) under different temperatures

	423K	473K	523K	573K	623K	673K	723K
k_1	4.72×10^7	4.47×10^7	4.25×10^7	4.06×10^7	3.89×10^7	3.74×10^7	3.61×10^7
k_{-1}	3.01×10^{-16}	8.07×10^{-14}	7.39×10^{-12}	3.06×10^{-10}	6.94×10^{-9}	9.88×10^{-8}	9.72×10^{-7}
k_2	1.18×10^8	1.11×10^8	1.06×10^8	1.01×10^8	9.70×10^8	9.34×10^7	9.00×10^7
k_{-2}	1.59×10^4	3.85×10^4	7.85×10^4	1.40×10^5	2.29×10^5	3.45×10^5	4.90×10^5
k_3	1.62×10^{-1}	2.91×10^0	2.99×10^1	2.04×10^2	1.02×10^3	4.02×10^3	1.31×10^4
k_{-3}	2.32×10^5	2.64×10^5	2.92×10^5	3.17×10^5	3.37×10^5	3.52×10^5	3.63×10^5
k_4	9.08×10^{-6}	8.04×10^3	3.04×10^{-2}	6.12×10^{-1}	7.67×10^0	6.63×10^1	4.27×10^2
k_{-4}	3.21×10^{-1}	3.66×10^{-1}	4.13×10^{-1}	4.65×10^{-1}	5.21×10^{-1}	5.81×10^{-1}	6.48×10^{-1}
k_5	7.58×10^{-3}	3.30×10^{-1}	6.99×10^0	8.68×10^1	7.19×10^2	4.35×10^3	2.05×10^4
k_6	1.10×10^1	2.74×10^2	3.69×10^3	3.17×10^4	1.93×10^5	8.97×10^5	3.38×10^6
k_{-6}	9.76×10^6	1.43×10^7	2.10×10^7	3.06×10^7	4.47×10^7	6.50×10^7	9.45×10^7
k_7	7.02×10^6	4.41×10^7	1.97×10^8	6.82×10^8	1.95×10^9	4.78×10^9	1.04×10^{10}
k_8	2.09×10^{-4}	1.37×10^{-2}	4.01×10^{-1}	6.45×10^0	6.62×10^1	4.79×10^2	2.63×10^3
k_{-8}	1.12×10^{13}	1.39×10^{13}	1.72×10^{13}	2.13×10^{13}	2.63×10^{13}	3.24×10^{13}	4.01×10^{13}
k_9	5.26×10^4	3.53×10^5	1.64×10^6	5.84×10^6	1.70×10^7	4.20×10^7	9.18×10^7
k_{-9}	2.13×10^{-5}	2.24×10^{-5}	2.39×10^{-5}	2.54×10^{-5}	2.71×10^{-5}	2.89×10^{-5}	3.08×10^{-5}
k_{10}	1.06×10^8	3.88×10^8	1.11×10^9	2.65×10^9	5.51×10^9	1.03×10^{10}	1.76×10^{10}
k_{11}	8.75×10^{10}	3.58×10^{11}	1.10×10^{12}	2.75×10^{12}	5.89×10^{12}	1.12×10^{13}	1.93×10^{13}

Table S21. Equilibrium coverages (θ , ML) of all species when $p_{\text{H}_2\text{O}}/p_{\text{CO}}=4$ under different temperatures on the NiCo(111) surface

	423 K	473 K	523 K	573 K	623 K	673 K	723 K
θ_{CO^*}	6.91×10^{-2}	6.93×10^{-2}	6.98×10^{-2}	7.05×10^{-2}	7.10×10^{-2}	7.11×10^{-2}	7.11×10^{-2}
$\theta_{\text{H}_2\text{O}^*}$	9.31×10^{-1}	9.31×10^{-1}	9.30×10^{-1}	9.29×10^{-1}	9.28×10^{-1}	9.26×10^{-1}	9.21×10^{-1}
θ_{OH^*}	2.00×10^{-8}	3.05×10^{-7}	2.75×10^{-6}	1.46×10^{-5}	3.80×10^{-5}	5.77×10^{-5}	7.01×10^{-5}
θ_{H^*}	2.00×10^{-8}	3.05×10^{-7}	2.75×10^{-6}	1.46×10^{-5}	3.80×10^{-5}	5.77×10^{-5}	7.01×10^{-5}
θ_{O^*}	3.10×10^{-15}	1.01×10^{-12}	1.13×10^{-10}	5.76×10^{-9}	1.59×10^{-7}	2.69×10^{-6}	3.05×10^{-5}
θ_{COOH^*}	3.61×10^{-14}	8.13×10^{-12}	2.39×10^{-10}	1.41×10^{-9}	7.65×10^{-9}	4.83×10^{-8}	2.07×10^{-7}
θ_{CHO^*}	5.47×10^{-21}	4.05×10^{-18}	6.95×10^{-16}	3.10×10^{-14}	3.79×10^{-13}	2.20×10^{-12}	9.12×10^{-12}
θ_{HCOO^*}	2.33×10^{-42}	1.55×10^{-35}	3.66×10^{-30}	5.18×10^{-26}	6.68×10^{-23}	2.07×10^{-20}	2.79×10^{-18}
$\theta_{\text{CO}_2^*}$	2.27×10^{-15}	2.34×10^{-12}	5.04×10^{-10}	2.43×10^{-8}	4.52×10^{-7}	5.25×10^{-6}	4.45×10^{-5}
$\theta_{\text{H}_2^*}$	3.05×10^{-12}	4.14×10^{-9}	1.18×10^{-6}	7.43×10^{-5}	8.26×10^{-4}	2.98×10^{-3}	7.07×10^{-3}
θ_*	2.22×10^{-16}	2.80×10^{-12}	2.77×10^{-10}	1.34×10^{-8}	2.25×10^{-7}	2.57×10^{-6}	4.52×10^{-6}

Table S22. Equilibrium coverages (θ , ML) of all species when $p_{\text{H}_2\text{O}}/p_{\text{CO}} = 4$ under different temperatures on the NiCu(111) surface

	423 K	473 K	523 K	573 K	623 K	673 K	723 K
θ_{CO^*}	9.14×10^{-2}	9.18×10^{-2}	9.24×10^{-2}	9.35×10^{-2}	9.50×10^{-2}	9.69×10^{-2}	9.88×10^{-2}
$\theta_{\text{H}_2\text{O}^*}$	9.09×10^{-1}	9.08×10^{-1}	9.08×10^{-1}	9.06×10^{-1}	9.05×10^{-1}	9.03×10^{-1}	9.00×10^{-1}
θ_{OH^*}	7.16×10^{-10}	1.37×10^{-8}	1.50×10^{-7}	1.09×10^{-6}	5.84×10^{-6}	2.41×10^{-5}	7.98×10^{-5}
θ_{H^*}	7.16×10^{-10}	1.37×10^{-8}	1.46×10^{-7}	9.49×10^{-7}	3.51×10^{-6}	7.62×10^{-6}	1.20×10^{-5}
θ_{O^*}	2.10×10^{-23}	3.77×10^{-20}	1.65×10^{-17}	2.58×10^{-15}	1.84×10^{-13}	7.15×10^{-12}	1.69×10^{-10}
θ_{COOH^*}	3.34×10^{-16}	1.58×10^{-13}	2.30×10^{-11}	1.36×10^{-9}	3.69×10^{-8}	5.00×10^{-7}	4.62×10^{-6}
θ_{CHO^*}	2.38×10^{-22}	8.92×10^{-20}	9.46×10^{-18}	3.88×10^{-16}	6.85×10^{-14}	7.52×10^{-14}	1.15×10^{-11}
θ_{HCOO^*}	2.92×10^{-47}	1.32×10^{-40}	2.91×10^{-35}	6.57×10^{-31}	2.14×10^{-27}	1.65×10^{-24}	1.69×10^{-21}
$\theta_{\text{CO}_2^*}$	1.32×10^{-19}	5.00×10^{-16}	4.15×10^{-13}	1.07×10^{-10}	1.08×10^{-8}	4.31×10^{-7}	7.24×10^{-6}
$\theta_{\text{H}_2^*}$	2.08×10^{-14}	3.07×10^{-11}	1.08×10^{-8}	1.15×10^{-6}	3.41×10^{-5}	3.09×10^{-4}	1.33×10^{-3}
θ_*	4.38×10^{-6}	1.32×10^{-5}	3.26×10^{-5}	6.90×10^{-5}	1.22×10^{-4}	1.45×10^{-4}	7.70×10^{-4}

On the basis of DFT calculated results, a microkinetic modeling of WGS reaction over NiCo(111) and NiCu(111) surfaces are carried out. Initial coverage of CO, H₂O and vacancies are set as 0, 0 and 1 ML (**Table S16**). The range from 423K to 723K are chosen to be calculated, which is consistent with the temperature range of the WGS reaction catalysts. In **Fig. S18a-b**, on both NiCo(111) and NiCu(111) surfaces, under the same temperature, the equilibrium coverages of CO (θ_{CO^*}) gradually decrease, $\theta_{\text{H}_2\text{O}^*}$ gradually increase with the rise of $p_{\text{H}_2\text{O}}/p_{\text{CO}}$ till $p_{\text{H}_2\text{O}}/p_{\text{CO}} = 4$. When either θ_{CO^*} or $\theta_{\text{H}_2\text{O}^*}$ keeps nearly a constant. In fact, experimentally, the $p_{\text{H}_2\text{O}}/p_{\text{CO}}$ ratio is often less than 4,^{5,7} which is in line with the above analysis. At $p_{\text{H}_2\text{O}}/p_{\text{CO}}=4$, as the operating temperature increases, all the vacancies

of NiCo (111) and NiCu(111) surfaces are nearly occupied by reactive species ($\theta_{\text{H}_2\text{O}^*}$), θ^* remains close to 0, θ_{CO^*} remain close to 0.06ML and 0.09 ML on the NiCo (111) and NiCu(111) surfaces, respectively, which are helpful to avoid CO depositing and catalyst poisoning. In summary, this indicates that NiCo (111) and NiCu(111) are favorable for avoiding CO deposition. And the pressure ratio $p_{\text{H}_2\text{O}}/p_{\text{CO}} \leq 4$ is found to be the favorable operating condition for WGS reaction on NiCo(111) and NiCu(111) surfaces. In **Fig. S18c**, the reaction rate on the NiCo (111) increase from -7.82 to $1.34 \text{ s}^{-1} \cdot \text{site}^{-1}$, the reaction rate on the NiCu (111) increase from -14.79 to $0.50 \text{ s}^{-1} \cdot \text{site}^{-1}$ with the increase in temperature (from 423 to 723 K), which suggests that the reaction activity improves with the temperature. The comparison clearly shows that at the same temperature, the reaction rate on NiCo (111) is larger than NiCu (111) surface. These indicate the higher catalytic activity of NiCo (111), followed by NiCu (111) surface.

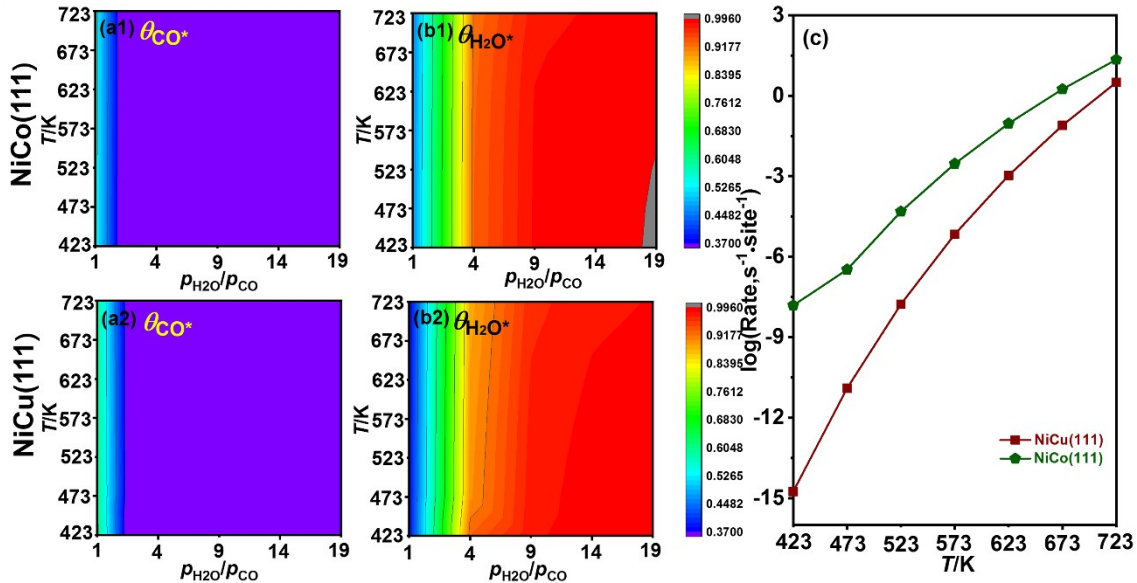


Fig. S18. (a) CO coverages (θ_{CO^*}), (b) H₂O coverages ($\theta_{\text{H}_2\text{O}^*}$) as a function of $p_{\text{H}_2\text{O}}/p_{\text{CO}}$ and temperature; (c) The WGS reaction rate ($\text{s}^{-1} \cdot \text{site}^{-1}$) from calculated studies when $p_{\text{H}_2\text{O}}/p_{\text{CO}} = 4:1$ on NiCo (111) and NiCu(111) surfaces.

9. Experimental details

9.1. Materials

$\text{Ni}(\text{NO}_3)_2 \cdot 6\text{H}_2\text{O}$, $\text{Co}(\text{NO}_3)_2 \cdot 6\text{H}_2\text{O}$, $\text{Cu}(\text{NO}_3)_2 \cdot 3\text{H}_2\text{O}$, $\text{Fe}(\text{NO}_3)_3 \cdot 9\text{H}_2\text{O}$, $\text{Al}(\text{NO}_3)_3 \cdot 9\text{H}_2\text{O}$, $\text{Zn}(\text{NO}_3)_2 \cdot 6\text{H}_2\text{O}$ and urea are bought from Sigma Aldrich and are used without further purification. Quartz sand (SiO_2 , 40-60 mesh) is purchased from Tianjin Guangfu Fine Chemical Research Institute, and wash is performed using concentrated HCl before used. Deionized (DI) water with resistivity 18.2 $\text{M}\Omega \cdot \text{cm}$ is used in all experimental processes.

9.2. Synthesis of NiAl-LDH and NiMAl-LDH (M=Cu, Co, Fe Zn) precursors

The Ni_2Al_1 -LDHs precursors are prepared by a facile urea decomposition method. Typically, $\text{Ni}(\text{NO}_3)_2 \cdot 6\text{H}_2\text{O}$ (0.08 M), $\text{Al}(\text{NO}_3)_3 \cdot 9\text{H}_2\text{O}$ (0.04 M) and urea (0.5 M) are dissolved in 500 mL deionized water. The mixed solution is stirred at room temperature for 3 h, followed by aging in a sealed Teflon autoclave at 110 °C for 12 h. The resulting precipitate is separated, followed by washed with DI water thoroughly and dried for 12 h at 60 °C. $\text{Ni}_1\text{Co}_1\text{Al}_1$ -LDHs, $\text{Ni}_1\text{Cu}_1\text{Al}_1$ -LDHs, $\text{Ni}_1\text{Fe}_1\text{Al}_1$ -LDHs and $\text{Ni}_1\text{Zn}_1\text{Al}_1$ LDHs were synthesized based on a similar method described above in addition to replacing a portion of the $\text{Ni}(\text{NO}_3)_2 \cdot 6\text{H}_2\text{O}$ with other metal nitrate.

9.3. Synthesis of supported Ni and NiM-bimetallic alloys catalysts

The above LDH precursors are reduced in a H_2/N_2 (1/9, v/v) stream at various temperatures (500 °C) for 6 h (heating rate: 2 °C min⁻¹). This reduction process leads to the structural transformation from LDH precursors to monometallic Ni or NiM-bimetallic alloys catalysts. Finally, the as-obtained

product is cooled to room temperature in a N₂ stream.

9.4. Catalytic evaluations

The catalytic performances of as-synthesis samples toward the WGS reaction are carried out in a fix-bed reactor with a stainless-steel tube of interior diameter is 10 mm at atmospheric pressure. Prior to the catalytic reaction, 300 mg LDH with 40-60 mesh mixed equal volume of quartz is pretreated in H₂ atmosphere (20.0 volume % H₂/N₂ mixture, 50 ml min⁻¹, 500 °C, 2 h). For the catalytic performance tests, the water is injected into the reaction system by using a syringe pump at a rate of 0.02⁻¹ mL min⁻¹ and mixed with CO (6.25 ml/min) and He gas (70 ml min⁻¹) within 210-330 °C. The stability evaluation was performed under the same reaction conditions. The products are analysed online by using a gas chromatograph (Shimadzu, GC-17A) with TCD detectors equipped with TDX-01 column. CO conversion (X) and product yield are calculated as followed.

$$X_{CO} = \frac{F_{CO, in} - F_{CO,out}}{F_{CO, in}} \times 100\% \quad (S11)$$

$$S_{C_i} = \frac{F_{C_i, out}}{F_{CO, in}} \times 100\% \quad (S12)$$

$F_{CO,in/out}$ is the molar flow rate of ethanol at the inlet/outlet of the reactor, respectively. F_{C_i} denotes the molar flow rate of C-containing product (CO₂ and CH₄) at the reactor outlet, respectively.

9.5. Characterization

Powder X-ray diffraction (XRD) is carried out on a Rigaku XRD-6000 diffractometer with Cu Ka radiation ($\lambda = 0.15418$ nm). The Zeiss Supra 55 scanning electron microscope (SEM) is applied to analyze the morphology of the samples. Transmission electron microscopy (TEM) images are

collected by using a JEOL JEM-2010 high-resolution transmission electron microscope. X-ray photoelectron spectroscopy (XPS) analysis is carried out on an AXIS SUPRA X-ray photoelectron spectrometer (pressure: 2×10^{-9} Torr) using an Al K α X-ray source.

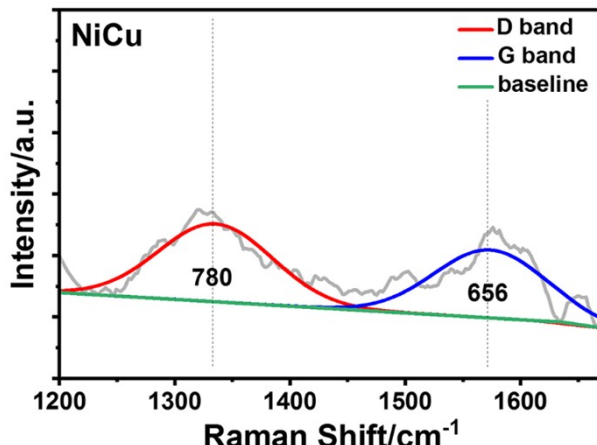


Fig. S19. Raman spectrum collected in air on the surface of used NiCu alloy.

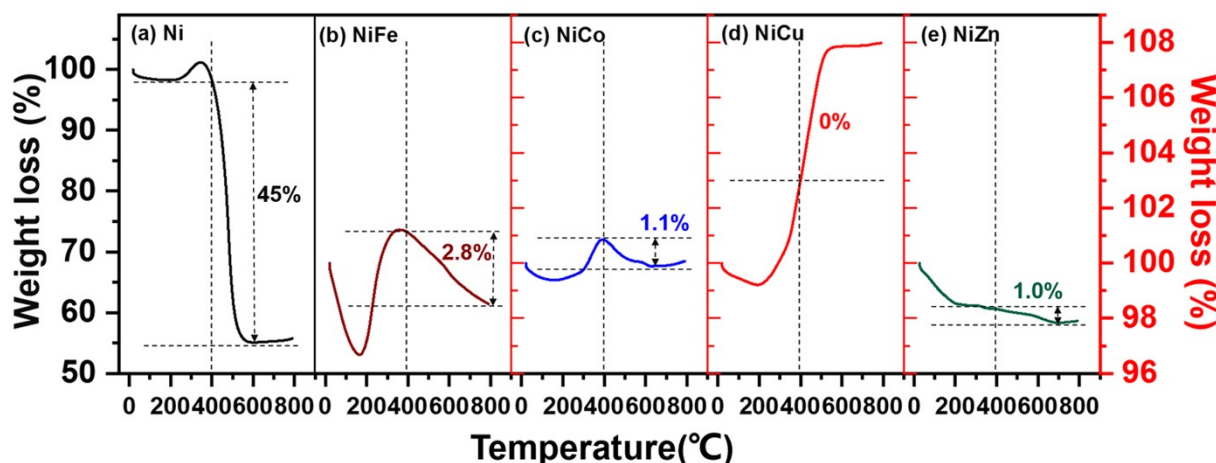


Fig. S20. Thermogravimetric (TG) analysis results of used (a) Ni, (b) NiFe, (c) NiCo, (d) NiCu and (d) NiZn samples after 25 h long time test.

10. References

- (S1) J.-H. Lin, V. V. Gulians. *ChemCatChem* 2012, **4**, 1611–1621.
- (S2) L. F. Chen, W. Liu, H. S. Feng, Y. Y. Ren, C. Y. Chen, S. Wang, P. Yin, Y. S. Yang, X. Zhang, M. Wei. *Catal. Sci. Technol.* 2021, **11**, 4376–4386.
- (S3) X. W. Liu, C. F. Huo, Y. W. Li, J. G. Wang, H. J. Jiao. *Surf. Sci.* 2012, **606**, 733–739.

- (S4) T. Ossowski, J. L. F. Da Silva, A. Kiejna. *Surf. Sci.* 2018, **668**, 144–149.
- (S5) A. Chakrabarty, O. Bouhali, N. Mousseau, C. S. Becquart, F. El-Mellouhi. *J. Chem. Phys.*, 2016, **145**, 044710.
- (S6) U. K. Chohan, E. Jimenez-Melero, S. P. K. Koehler, *Appl. Surf. Sci.* 2016, **387**, 385–392.
- (S7) K. Iokibe, K. Azumi, H. Tachikawa. *J. Phys. Chem. C* 2007, **111**, 13510–13516.
- (S8) C.-H. Lin, C.-L. Chen, J.-H. Wang. *J. Phys. Chem. C* 2011, **115**, 18582–18588.
- (S9) S.-C. Huang, C.-H. Lin, J.-H. Wang. *J. Phys. Chem. C* 2010, **114**, 9826–9834.
- (S10) R. C. Catapan, A. A. M. Oliveira, Y. Chen, D. G. Vlachos. *J. Phys. Chem. C* 2012, **116**, 20281–20291.
- (S11) G. Kresse, J. Hafner. *Phys. Rev. B* 1993, **47**, 558–561.
- (S12) G. Kresse, J. Hafner. *Phys. Rev. B* 1994, **49**, 14251–14269.
- (S13) G. Kresse, J. Furthmuller. *Comput. Mater. Sci.* 1996, **6**, 15–50.
- (S14) G. Kresse, J. Furthmuller. *Phys. Rev. B* 1996, **54**, 11169–11186.
- (S15) Y. Pan, H. Zhang, D. Shi, J. Sun, S. Du, F. Liu, H.-J. Gao. *Adv. Mater.* 2009, **21**, 2777–2780.
- (S16) P. E. Blöchl. *Phys. Rev. B* 1994, **50**, 17953.
- (S17) G. Henkelman, B. P. Uberuaga, H. Jónsson, *J. Chem. Phys.* 2000, **113**, 9901–9904.
- (S18) G. Henkelman, H. Jónsson. *J. Chem. Phys.* 2000, **113**, 9978–9985.
- (S19) Q.-X. Cai, J.-G. Wang, Y.-G. Wang, D. H. Mei. *AIChE J.* 2015, **61**, 3812–3824.
- (S20) O. Deutschmann, R. Schmidt, F. Behrendt, J. Warnatz. *Combust. Inst.* 1996, **1**, 1747–1754.
- (S21) T. N. Le, B. Liu, L. K. Huynh. *J. Comput. Chem.* 2014, **35**, 1890–1899.
- (S22) H. Liu, R. Zhang, L. Ling, Q. Wang, B. Wang, D. Li. *Catal. Sci. Technol.* 2017, **7**, 3758–3776.
- (S23) L. Xu, D. Mei, G. Henkelman. *J. Chem. Phys.* 2009, **131**, 244520–244528.
- (S24) T. N. Le, B. Liu, L. K. Huynh, *J. Comput. Chem.* 2014, **35**, 1890–1899.
- (S25) B. Hammer, J. K. Nørskov. *Surf. Sci.* 1995, **343**, 211–220.
- (S26) B. Hammer, J. K. Nørskov. *Adv. Catal.* 2000, **45**, 71.